General Disclaimer

One or more of the Following Statements may affect this Document

- This document has been reproduced from the best copy furnished by the organizational source. It is being released in the interest of making available as much information as possible.

- This document may contain data, which exceeds the sheet parameters. It was furnished in this condition by the organizational source and is the best copy available.

- This document may contain tone-on-tone or color graphs, charts and/or pictures, which have been reproduced in black and white.

- This document is paginated as submitted by the original source.

- Portions of this document are not fully legible due to the historical nature of some of the material. However, it is the best reproduction available from the original submission.

Produced by the NASA Center for Aerospace Information (CASI)

UCLA-ENG-8073

VAPOR - LIQUID PHASE SEPARATOR

T.H.K. Frederking, Principal Investigator
G.S. BROWN, C. CHUANG, Y. KAMIOKA,
Y.I. KIM, JEFFREY MARSHALL LEE, S.W.K. YUAN

SCHOOL OF ENGINEERING AND APPLIED SCIENCE
UNIVERSITY OF CALIFORNIA, LOS ANGELES
90024 CA

FINAL REPORT

VAPOR-LIQUID   PHASE   SEPARATOR

T.H.K. Frederking, Principal Investigator
G.S. Brown, C. Chuang , Y. Kamioka , Y.I.
Kim , Jeffrey Marshall Lee, S.W.K. Yuan

SCHOOL OF ENGINEERING AND APPLIED SCIENCE
UNIVERSITY OF CALIFORNIA, LOS ANGELES

FINAL REPORT

PREPARED FOR

October   1980

ABSTRACT

Conceptual design and development work has considered porous plugs as vapor-liquid phase separators for He II storage vessels at reduced gravity, mostly in the form of passive devices with a constant area. Methods have been studied aiming at flow rate modifications by incorporation of components with variable cross sectional area. A particular device has been designed and constructed which uses a shutter-type system for area variation. This system has been tested successfully permitting flow rate changes of up to $\pm 60\%$ from its mean value.

KEYWORDS

Porous plugs as passive components

Vapor-liquid phase separator

Liquid He II

Variable-cross sectional area device

Mass throughput variation

Heat load modulation

PRECEDING PAGE BLANK NOT FILMED

TABLE OF CONTENTS

PRECEDING PAGE BLANK NOT FILMED

I. SUMMARY

In I.R. telescope systems operating at reduced gravity with liquid He II as a heat sink, flexible operation may be accomplished by incorporating variable impedances into the vapor-liquid phase separator. The latter is used in one family of systems at the He II vessel exit and the vent line entrance respectively. For more flexibility, porous plugs of fixed geometry may be replaced by devices of variable impedances. They may require tight tolerances. Another approach relies on devices with variable area of the flow cross section in conjunction with plugs. In the last 30 years industrial production of plugs with sufficient reliability has been extended from the 10 to the 1 μm pore size range. This permits more freedom in design approaches relying on porous plugs.

In the present report, design studies in this field of variable-area devices are outlined. One particular design, a rotatable shutter device has been implemented and tested at He II temperatures. The proof-of principle experiment is described. From the tests it is concluded that this approach is suitable for the enlargement of the range of operation of I.R. telescope equipment subjected to varying degrees of dissipation rates and resulting entropy rejection to the coolant.

1

II. INTRODUCTION

Liquid - vapor interfaces and related phenomena at reduced gravity have received considerable attention for the preparation of current and future space missions. The porous plug, in particular, has been studied as a phase separation device for superfluid liquid helium II vessels. The latter may serve as coolant baths for IR telescopes[1]. The porous plug is located at the vent line entrance which is to be the boundary of the liquid of the storage vessel. Thus, one function of the plug is to maintain a well-defined vapor liquid interface. Another function of the plug is to provide for a controlled throughput of mass and entropy through the channels of the porous media. The reduced gravity forces of space operation make it possible to keep the He II confined to its dewar without exerting strong forces across the plug. On the down-stream side of the plug the vent line carries cold He^4 gas through radiation shields. The latter in turn keep the external heat load on the liquid vessel small. Any departure of the liquid drainage rate toward the high or the low side of the design throughput is undesired once permitted design tolerances are exceeded. A fixed-geometry plug however has only a limited degree of

flexibility from the point of view of flow rate tolerances. Therefore solutions have become known which incorporate variable flow impedances at the exit of the tank. An example is the pin device with after-heater permitting vaporization of residual liquid [2)3)] . For this system relatively narrow tolerances are required. Further, additional entropy increases occur by heat supply downstream during vaporization of residual liquid. Therefore alternate solutions appear to be desirable . The present effort has been concerned with a device of variable cross sectional area available to the flow.
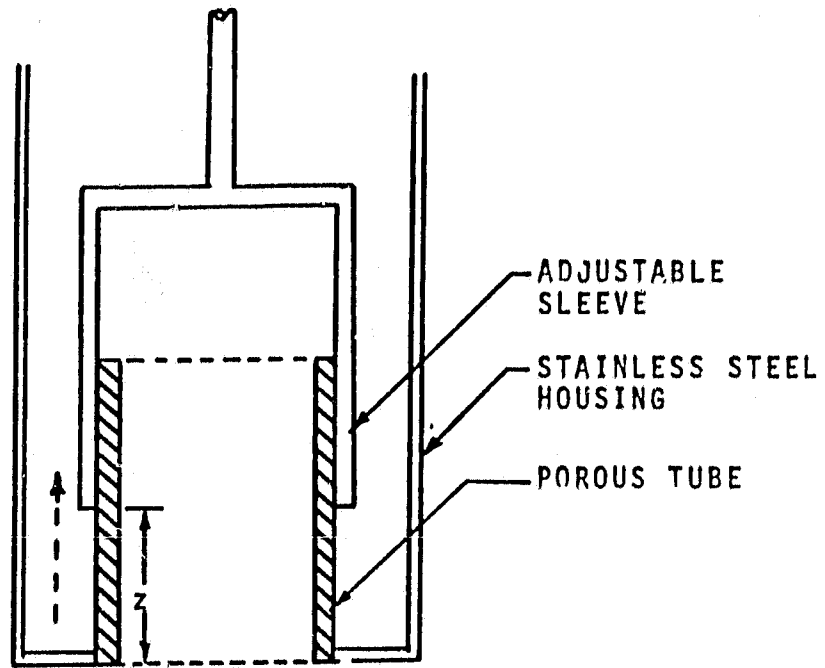
This report summarizes R & D work conducted in this area in collaboration with NASA , AMES Research Center. Initial design approaches are outlined in Section III . The particular solution selected for this project makes use of a porous stainless steel plug. In order to proceed to the manufacturing and testing phase, it appeared to be necessary to have sufficient plug geometry characterization. However, because of a lack of data this task has been restricted to a first order approach. Plug characterization efforts are reported in Section IV . Subsequently proof-of-principle runs were conducted which are described in Section V. Major points of the data discussion, a performance summary and conclusions are presented in Section VI.
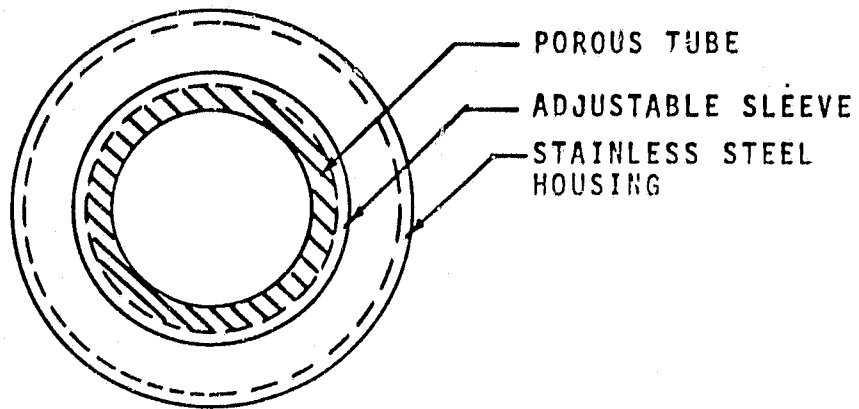
III . DESIGN OF VARIABLE AREA SYSTEMS

In comparison to pin devices[2)3)], a design approach
based on porous media requires knowledge of the plug system
to be used. In principle, a considerable degree of design
freedom appears to exist as powder metallurgy has been
developed to meet various demands for filter elements in
the processing industries.

Figure 1 depicts conceptually a sleeve system for a
porous cylinder. Figure 2 displays a shutter system based
on four circular porous disks. The shutter plate incorpo-
rates four void spaces. A change to a new angular position
coordinate produces a different cross sectional area avail-
able to He[4]. The present experiments, described subsequently,
have shown that the systems operational parameters are
changed considerably when "zero" flow cross section is
established. Therefore, the device with variable cross
section is not recommended as a shut-off valve, as far as
the present concept of a simple variable-area device is
concerned. Small holes arranged at strategic points in
the shutter plate may be used to establish minimum through-
put conditions.

Design consideration have included friction forces and
related dissipation created by movable parts and the drive
system respectively. Further, the range of the displacement

SIDE VIEW

- ADJUSTABLE SLEEVE
- STAINLESS STEEL HOUSING
- POROUS TUBE

TOP VIEW

- POROUS TUBE
- ADJUSTABLE SLEEVE
- STAINLESS STEEL HOUSING

Figure 1. Sleeve system for motion in axial direction;(Broken arrow : Mass flow direction; z = axial position coordinate).
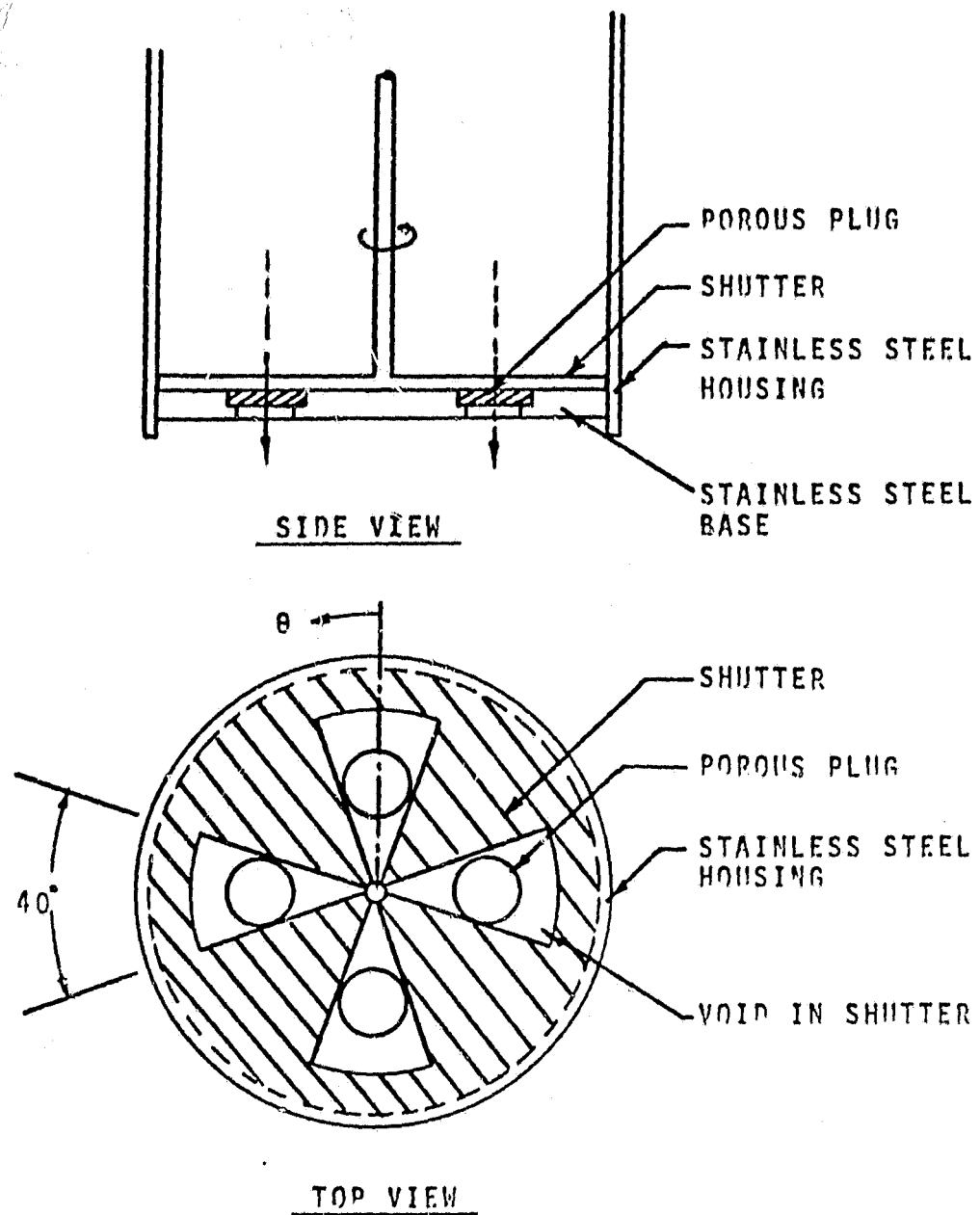
5

SIDE VIEW

TOP VIEW

Figure 2 . Shutter system based on circular porous disks;
(Broken arrow : Mass flow direction; θ variable
angular position coordinate).

6

coordinate, leakage aspects, type of motion, reliability, materials' machinability and economics have been assessed for the final choice. It turned out that for most attractive solutions, data of throughput versus displacement were unknown. Though several alternative designs are potentially attractive, the final choice adopted emphasized simplicity. This choice has been derived from various modifications of the scheme shown in Figure 2.

The system adopted is shown schematically in Figure 3. The rotatable shutter with an open cross section in the form of a semi-circle permits fluid access. Between the plug and the shutter, a flow control plate has a system of holes, again arranged in a semi-circular area. When the opening of the shutter is aligned with the hole system of the flow control plate, the maximum cross sectional area is available to transport. A position 180 degrees off this maximum cross sectional area is the position of minimum throughput. A small hole in the shutter dominates the minimum throughput of the system.

One point not mentioned so far is the location of the shutter with respect to the mass throughput. In principle a position upstream or downstream may be chosen. Downstream was preferred and implemented. This type of arrangement does not disturb the He II bath rapidly and

SHAFT

SHUTTER

FLOW CONTROL PLATE

PLUG

STAINLESS STEEL
HOUSING

SEMI-CIRCULAR
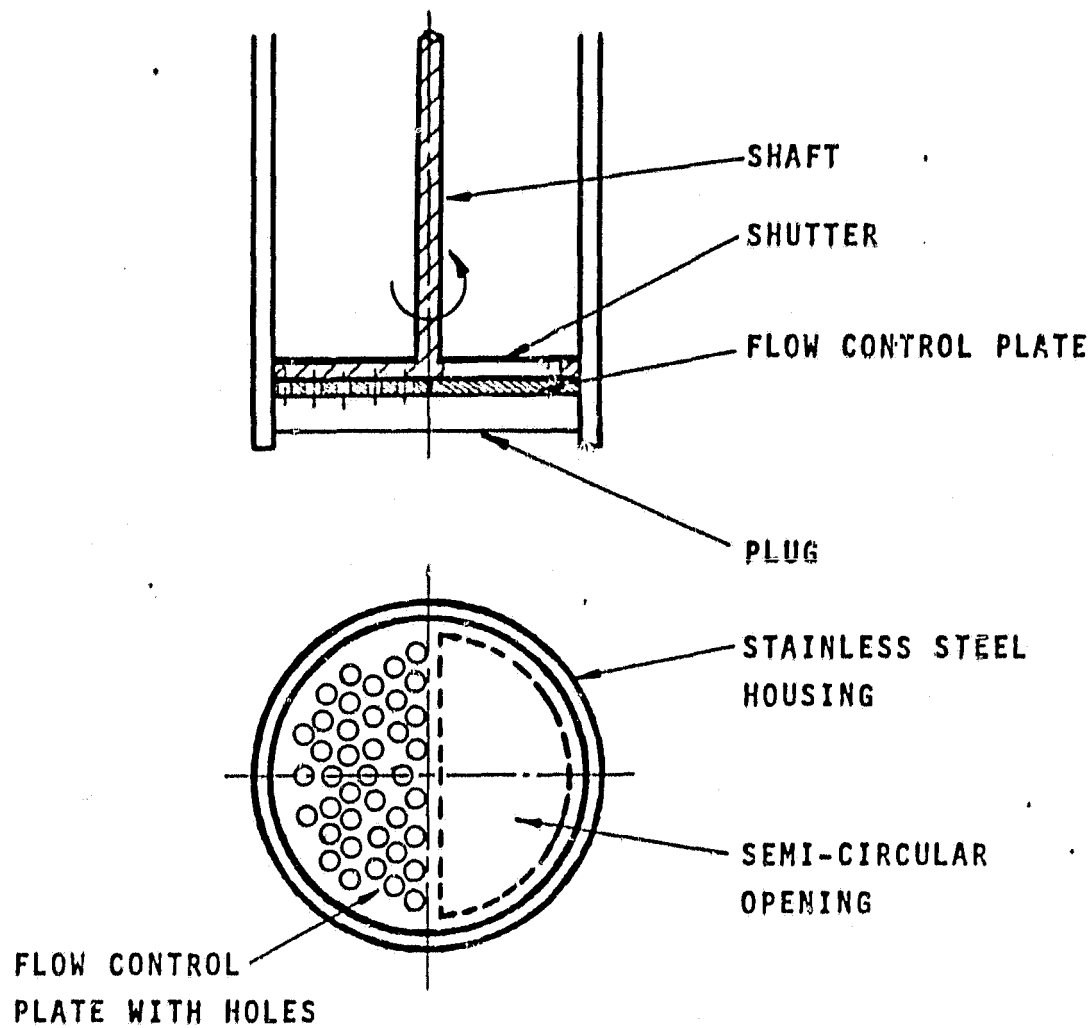OPENING

FLOW CONTROL
PLATE WITH HOLES

Figure 3 . Schematic of shutter system for a
variable-cross sectional area device

directly by dissipation processes resulting from friction

in the shutter and shutter drive system respectively.

IV. PLUG CHARACTERIZATION

EXPERIMENTS

Several measurements are useful for the characterization of porous media.However, a few methods(e.g.BET)introduce impurities and cause contamination of the plug. For this reason only a minimum of experiments were conducted in order to keep the plug clean and to maintain He^4 contact with the solid walls of the plug. Aside from plug identification tests, the main emphasis has been on permeability and a comparison with other plug data.

Plug identification. A surface profilometer is used to check details of the plug surface of the stainless steel plug manufacturer (Mott Metallurgical Corporation, Farmington, CO 06032). The stylus tip of the profilometer had a tip radius of 0.05 cm. Surface variations resolved at the resolution limit are of the order 0.3 μm. Records for three different stainless steel plugs are shown in Figures 4 to 6. During the runs the stylus is moved slowly across the plug, and the signal is displayed as a function of time on an X-Y-plotter (Houston Omnigraphic 2000). The signals of plugs of one particular manufacturer are seen to be sufficiently different. Thus, this simple method has some usefulness for plug identification.
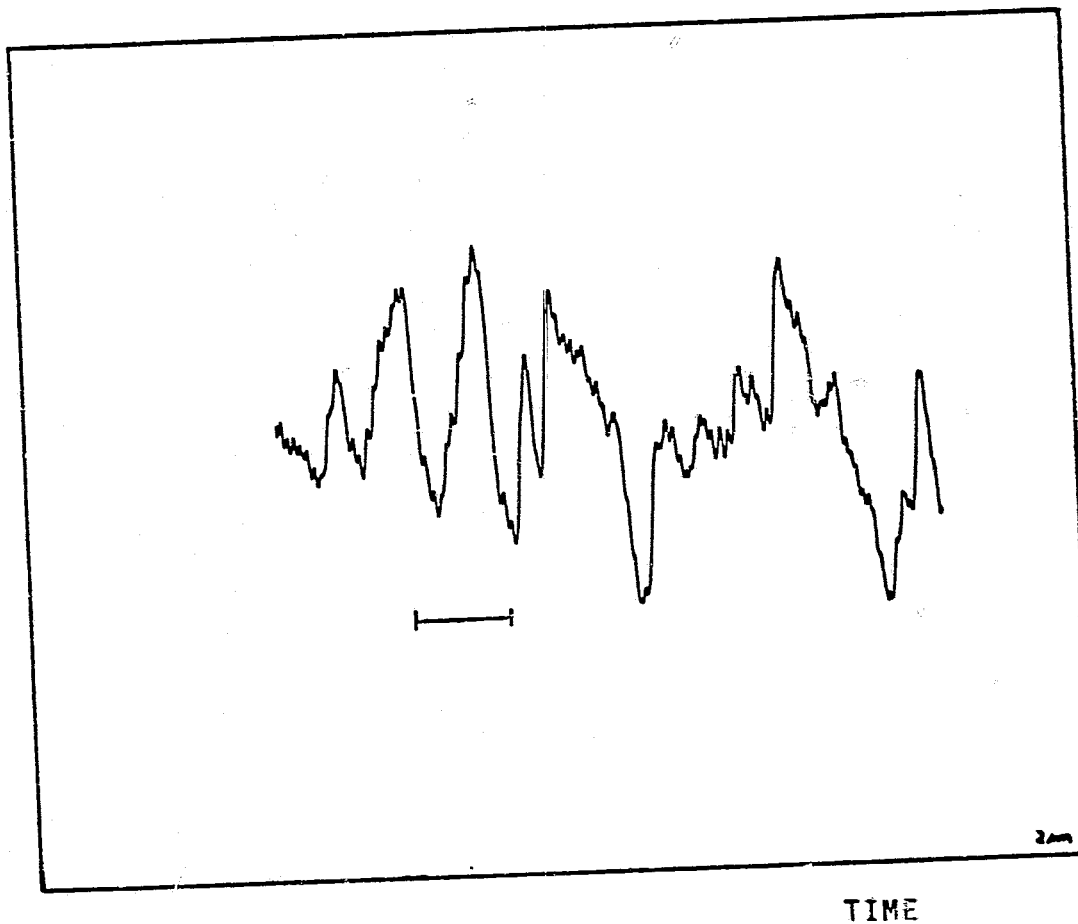
Figure 4.   Trace of 2 μm-plug (X-axis, Time scale : 1 unit = 1 sec; Unit length in vertical direction = 50 mV).

ARB.
UNITS

TIME
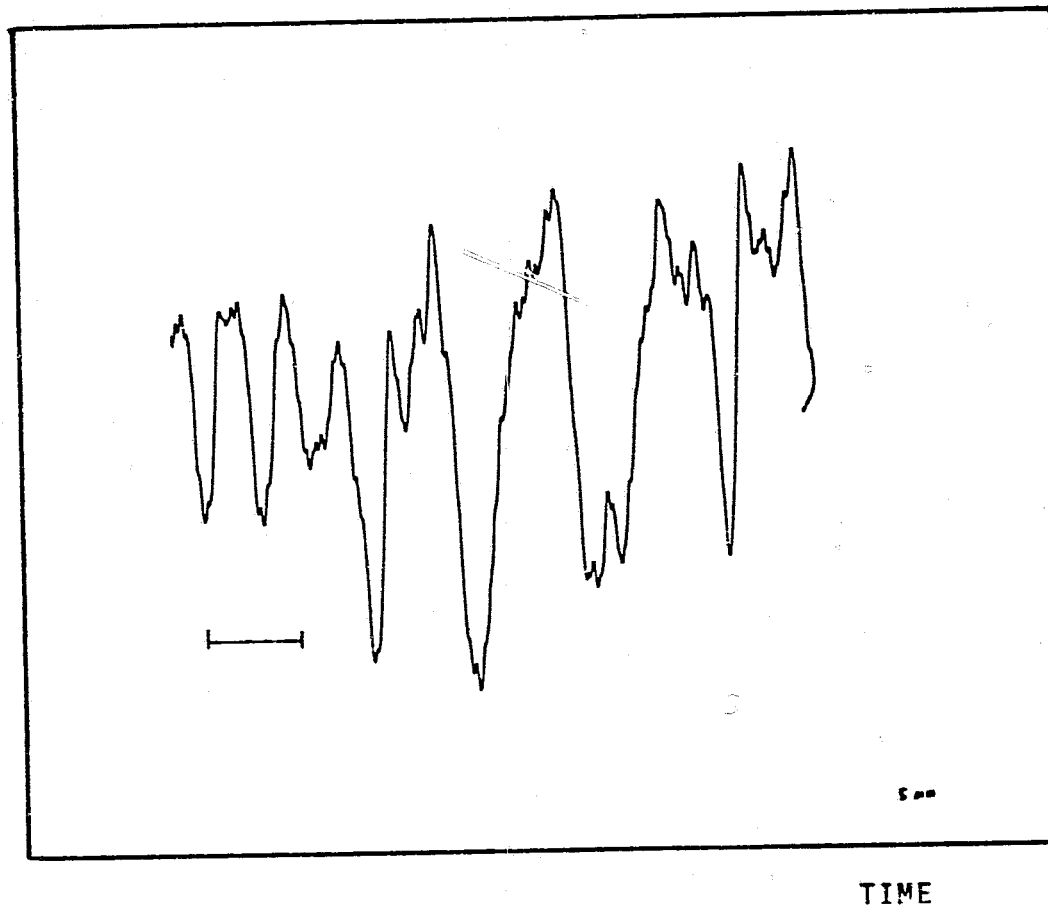
Figure 5.   Trace of ℓ μm-plug (X-axis, Time scale : 1 unit =
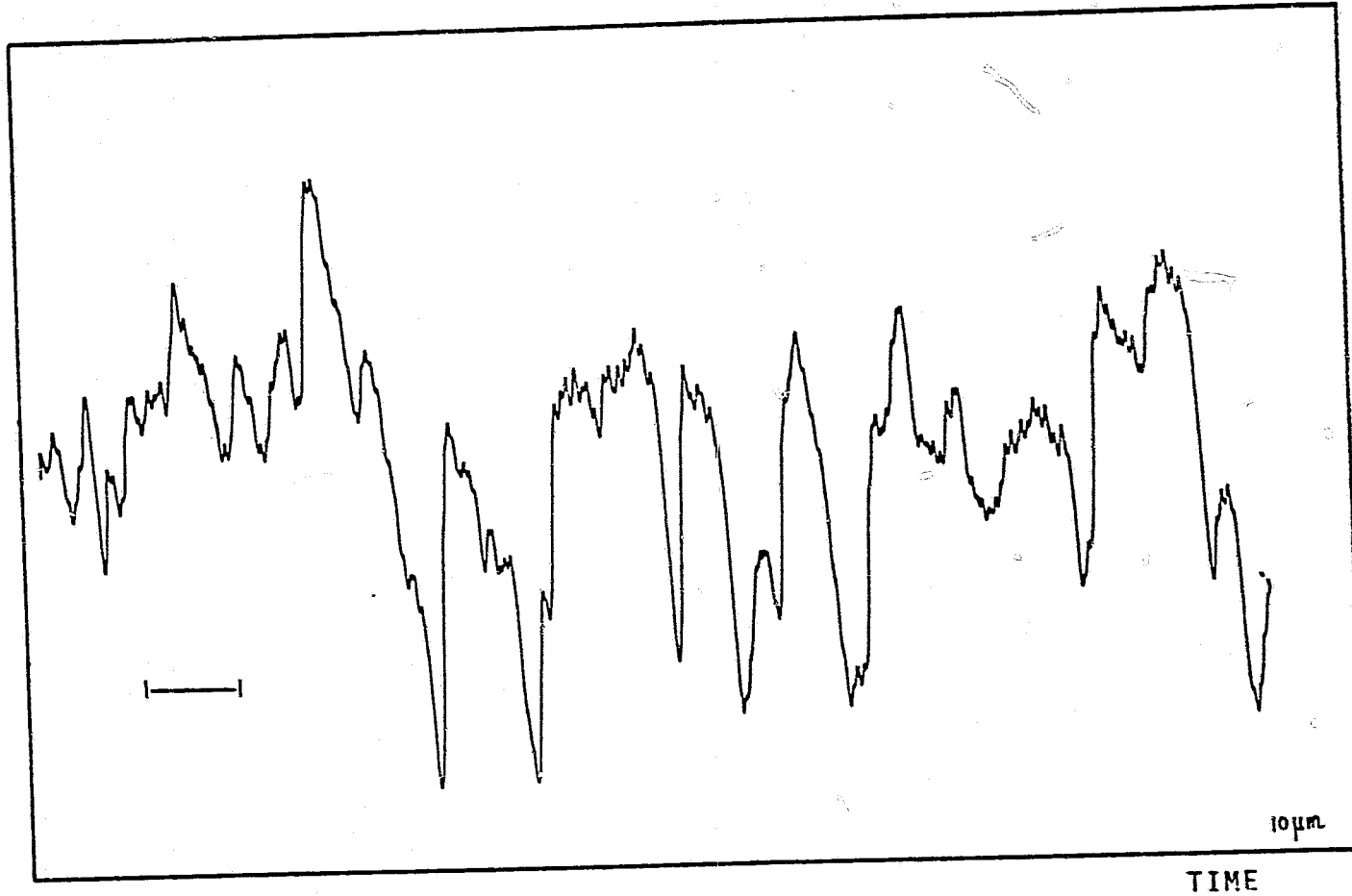   1 sec; Unit length in vertical direction = 50 mV).

Figure 6. Trace of 10 μm – plug; (X-axis, Time scale : 1 unit = 1 sec ;
Unit length in vertical direction = 50 mV).

Concepts. The quantity of prime interest for single-fluid (He[4]) – measurements has been the permeability (K_p) of Darcy's law

$$K_p = \overline{v_o}\, \eta\, / |\text{grad } P| \qquad (1)$$

(P pressure , $\overline{v_o}$ superficial velocity , η shear vis – cosity). For near-spherical particle systems undergoing a sintering process without a significant change in geometry, the special permeability model of Carman and Kozeny[4][5] is expected to be useful. This model predicts a permeability $(K_p)_{CK}$ as a function of the porosity (ε) and the particle radius (R_p)

$$(K_p)_{CK} = (36\, C_{CK})^{-1}\quad (2\, R_p)^2\quad \varepsilon^3/(1 - \varepsilon)^2 \qquad (2)$$

The Carman-Kozeny constant (C_{CK}) has a value around 5. Indeed the prefactor in Equation (2) of $(180)^{-1}$ has been shown to be a reasonable approximation for refractory metal plugs.[6]

There are two other categories of popular lengths in the discussion of plugs. One of them is the pore size (radius s_o). It is usually determined from bubble tests , i.e. contaminating tests. The other size is related to the throughput. For small flow rates in the laminar range, various versions of viscous flow equations are preferred, e.g. the Hagen-Poiseuille equation for capillary tubes :

$$\overline{v_o} = \mathcal{S}_o\, R_{hj}^2\, |\text{grad } P|\, / \eta \qquad (3)$$

One disadvantage of Equation (3) is the lack of any explicit reference to the porosity. Further there does not exist any generally accepted hydraulic radius R_{hj} in the literature on sintered plugs. A comparison of Equations (1) and (3) leads to a permeability

$$K_p = \zeta_o \cdot R_{hj}^2 \tag{4}$$

For concentric , circular cylinders the factor ζ_o in Equations (3) and (4) does not depart more than 25 % from the value 0.1 , as has been discussed elsewhere [6] .This property may be used for the definition of an ideal hydraulic radius for this kind of ducts of

$$(R_h)_{id} = (K_p / \zeta_o)^{1/2} \approx (K_p / 0.1)^{1/2} \tag{5}$$

A different R_h-value may be used to have a first order account of ε for sintered plugs

$$(R_h)_m = \left\{ \frac{K_p \varepsilon}{\zeta_o} \right\}^{1/2} \approx \left\{ \frac{K_p \varepsilon}{0.1} \right\}^{1/2} \tag{6}$$

At present however , the data scatter of literature results is larger than for packed bed data. Nevertheless, it is noted that in a restricted range of ε and pore sizes there should be proportionality between different lengths ,e.g. we have to first order

$$(K_p)^{1/2} \sim R_{hj} \sim s_o \tag{7}$$

Porosity data of sintered stainless steel plugs
are given in Table IV.1 . Various permeability data are
compared in Tables IV.2 and IV.3 . Further, Figure 7
compares specific results of non-metallic plugs with
refractory metal plugs.

Table IV. 1 lists porosities of stainless steel
plugs. The ϵ-values are seen to be below 50%. Table
IV. 2 indicates that the permeability of non-metallic
sintered plugs increases monotonically with pore size.
Table IV. 3 for sintered stainless steel plugs is at
variance with K_p- values of the preceding Table IV. 2.

There is only a limited support for relation (7).
Figure 7 displays $\sqrt{Kp}$ of references 8 and 9 and the data
of Table IV. 2. According to Equation (2), Darcy trans-
port is characterized by $[d \log \sqrt{K_p}/ d \log R_p]= 1$ for a
specified porosity. Figure 7 indicates data trends in
agreement with this power law exponent when the particle
radius is above 10 μm.

The other part of Figure 7 in the size range below
10 μm relates to $\sqrt{K_p}$ versus the (nominal) pore radius s_o.
The power law exponent $[d \log \sqrt{K_p}/ d \log s_o]$ for the data
of Table IV. 2 appears to be close to unity. However
in general there is no well-defined universal relationship
between s_o and R_p and an equivalent effective particle
radius respectively.

TABLE IV . 1

POROSITIES OF SINTERED STAINLESS STEEL PLUGS *

Plug No.	NOMINAL PORE SIZE s_o , μm	POROSITY ε
M2- ST 1	2	0.311
M2- ST 2	2	0.309
M2- ST 3	2	0.314
M5 - ST 4	5	0.328
M5 - ST 5	5	0.327
M5 - ST 6	5	0.326

*)

Determined by weight measurements and volume measurements .

TABLE IV.2. POROUS PLUG COMPARISON
(NON-METALLIC PLUGS)

NOMINAL PORE SIZE (Radius) s_0 , μm	MATERIAL	AUTHOR(S)	PERMEABILITY K_p , cm^2
1	Al-SILICATE	KLIPPING ET AL. [+*][7]	1.04×10^{-11}
5	$Al_2 O_3$	KARR-URBAN [**][8]	5.05×10^{-10}
10	GLASS	KLIPPING ET AL. [+*][7]	3.4×10^{-9}

----

*)

   Permeability based on throughput measurements at room
   temperature with dry air ;(I. Klipping, private communication).

**)

   Permeability data based on measurements with He^4 gas at 1 atm at
   room temperature ; (G.R. Karr, private communication).

+)

   Recalculated to be consistent with a permeability definition
   based on Darcy's law .

TABLE   IV.3. PLUG   DATA   COMPARISON
(STAINLESS   STEEL)

NOMINAL PORE SIZE s_o , μm	FLUID MEDIUM	PERMEABILITY K_p , cm^2	TEMPERATURE T , K	SOURCE
2 5 10	AIR (g)	$8 \cdot 10^{-9}$ $1.7 \cdot 10^{-8}$ $4.2 \cdot 10^{-8}$	T_{ROOM}	MOTT METALLURGICAL CORPORATION
2 2 2	He^4 (g)	$4.6 \cdot 10^{-9}$ $4.1 \cdot 10^{-9}$ $2 \cdot 10^{-9}$	T_{ROOM} 77 4.2	PRESENT RUNS *

*) Average of several runs with varying pressure difference
across plug ; (Data not representative of plug used in variable-
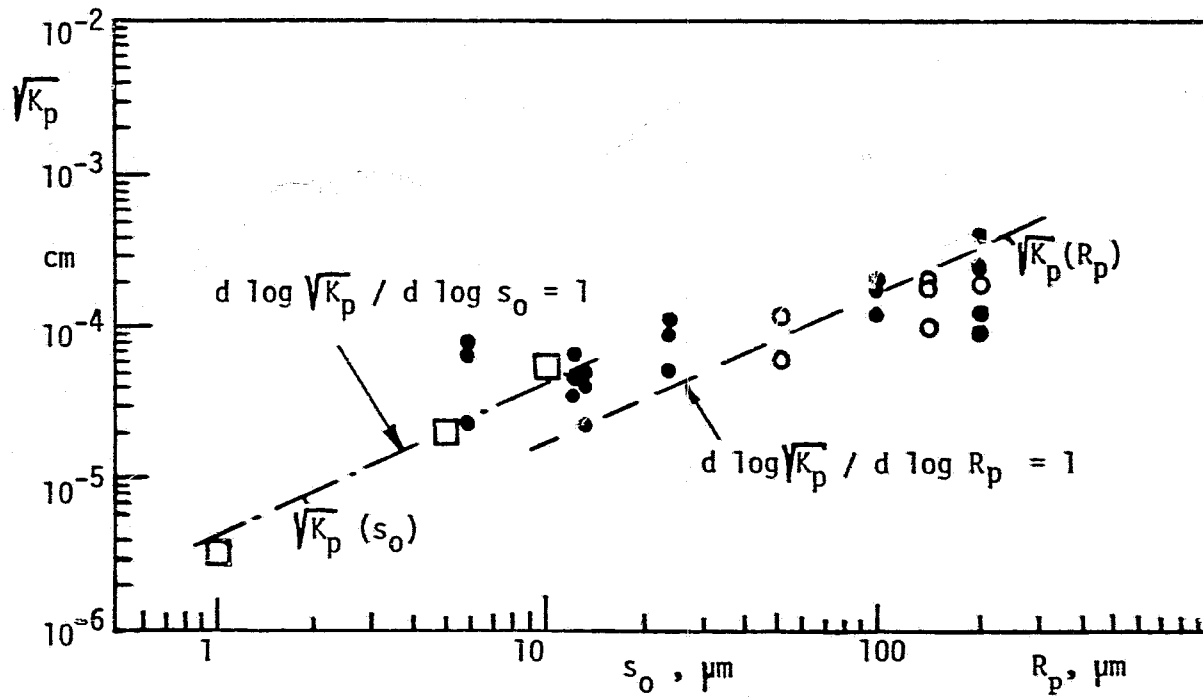area system).

Figure 7. Square root of the permeability versus nominal pore size (s_o) and particle radius R_p respectively; Squares: Sintered non-metallic plugs(Table IV .2); Open and full circles: Data of Hall[12] and Robinson [13] respectively for sintered tungsten.

Because of the lack of quantification of Equation (7) , a few open problem areas of plug characterization approaches are mentioned at this time:

First, a large number of surface variables at the fluid-solid interface may enter. They depend on manufacturing and plug preparation conditions.

Second, Knudsen transport ("Klinkenberg effect", mean free path effect) is expected to occur at localized very narrow flow passages. The extent of this contribution is in part a function of the sintering temperature .

Third,different adsorption conditions may exist when sintering and preconditioning before cooldown is modified. Minute amounts of impurities may have some influence (if they are present).

Despite these uncertainties, a rough assessment of the order of magnitude of K_p appears to be available from the information listed above. Thus, some crude design guide lines may be formulated. However, experimental data are required for quantification.

V. VARIABLE-AREA SYSTEM AND PROOF-OF-PRINCIPLE EXPERIMENT

System: Terrestrial simulation experiment. In any lab
simulation of phenomena at reduced gravity, a pump has to
replace the vacuum pumping conditions of space. The pump
has a characteristic performance surface, e.g. pressure
difference versus mass flow rate $\dot{m}$ and pump efficiency
as parameter. The "consumer" of power is the plug system.
Supply and consumption have to match during steady trans-
port. In other words, there is a well-defined point of
operation which is the intersection of the supply and
consumer function. At this point the pump's effective
pressure difference $(\Delta P)_{eff}$ is equal to the plug system's
pressure difference. The available $(\Delta P)_{eff}$ is a combina-
tion of the pump-produced pressure rise, line impedances
and ΔP-contributions from throttling components. Thus,
the available $(\Delta P)_{eff}$ and the related mass throughput
respectively characterize a particular lab system. It has
been proposed[9] to utilize the ratio of $\dot{m}$ to the parameter
(A_{tot} / L) of the plug as performance measure; (L = plug
length, A_{tot} = overall cross sectional area of the plug).
Values of ($\dot{m} L/A_{tot}$) are listed in Table V.1 at a tem-
perature of 1.7 K.

TABLE V. I . LABORATORY SYSTEM PERFORMANCE PARAMETERS

$$\dot{m} L / A_{tot} \quad at \quad 1.7 \quad K$$

NOMINAL PORE SIZE s_o , μm	MATERIAL	AUTHOR (S)	RATIO $\dot{m} L / A_{tot}$ mg / (s cm)
10	GLASS	KLIPPING ET AL . [7]	≈ 1.5
10	CERAMIC	PETRAC ET AL. [10]	≈ 0.6
5	CERAMIC	URBAN – KARR [8]	≈ 0.35
10	CERAMIC	URBAN ET AL. [9]	$\lesssim 0.1$
10	Ni	URBAN ET AL. [9]	$\lesssim 0.1$
1	CERAMIC	KLIPPING ET AL. [7]	$\lesssim 0.1$
2	STAINLESS STEEL	PRESENT EXPERIMENTS	$\lesssim 0.4$ (quasi–steady transport)

Our laboratory system is a modified version of the setup used by several investigators, e.g. Reference 9. Figure 8 shows essential components of our system. The outer He II bath simulates the vessel , the inner vent tube permits pumping of the vapor away from the plug. The latter separates the bath from the vent line. The rotatable shutter with semi-circular opening is designated as TS and made out of teflon . Low values of the coefficient of friction between teflon and brass have been found in other investigations [11] . The shutter is driven by a shaft extending downward from the motor M . The flow control plate (FCP) is made out of G-10 (thickness 0.1016 cm = 0.04 in.) This plate contains 40 holes with a hole diameter of 0.159 cm. A layer of glass microfibre paper is used as spacer between plug and FCP ; (Paper manufacturer : Whatman Ltd , grade GF/A , thickness 0.02 cm). The plug is mounted in a stainless steel tube holder using epoxy (Emerson & Cuming Inc., No. 1266). The inner diameter of the tube of alloy 304 is machined to 2.553 cm = 1.005 in., in order to accomodate the plug with an O.D. of 2.54 cm = 1 in.. The outer diameter of the tube has been machined to 2.67 cm (= 1.05 in) resulting in a wall thickness of 0.06 cm (alloy 304). Epoxy is used also to fix the location of the flow control plate. The holes in
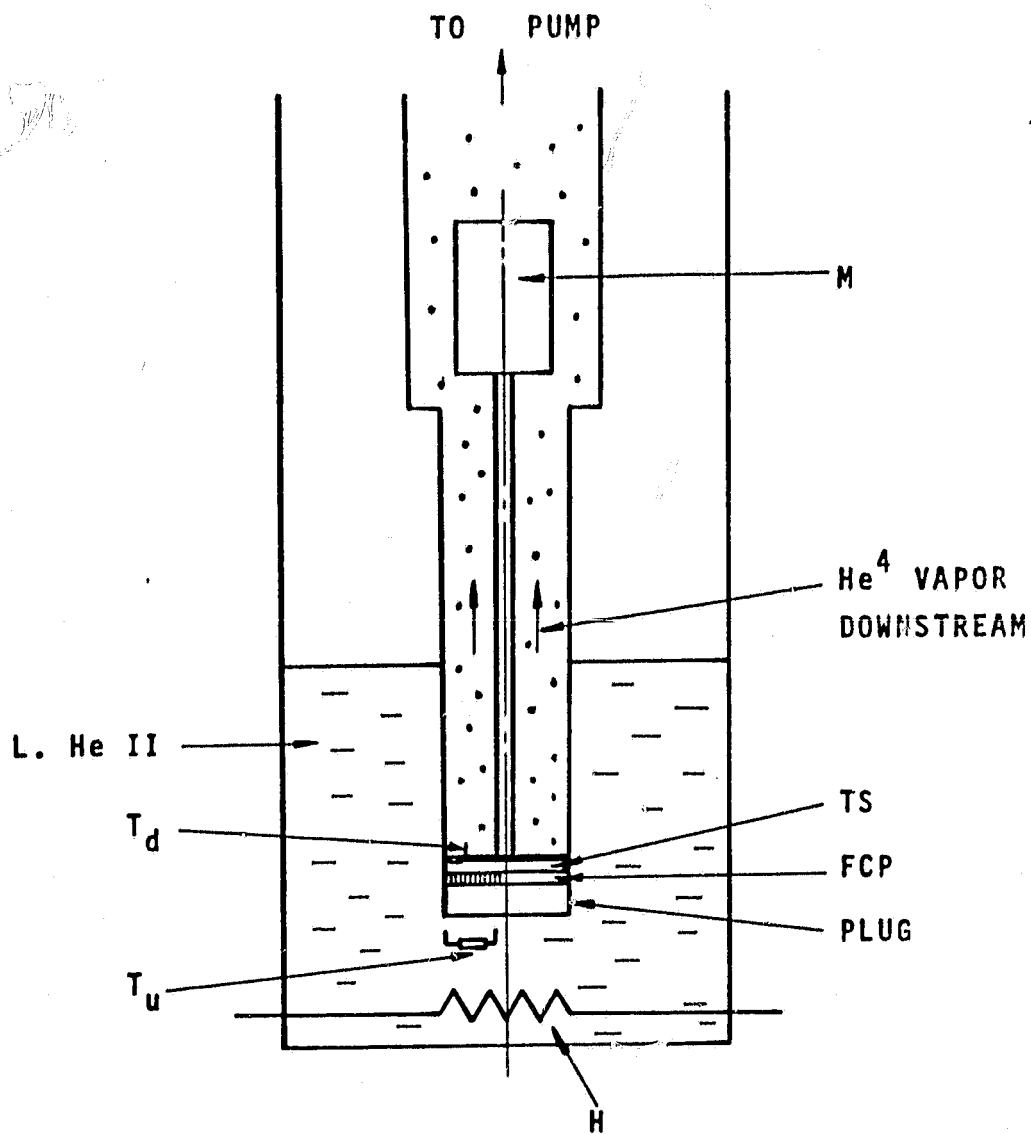
Figure 8.   Schematic of present laboratory system

the flow control plate are extended through the micro-fibre paper. Slow rotation of the shutter is established during the tests in order to separate various effects during the runs without excessive diagnostic difficulty. The d.c. motor (M) has a nominal voltage of 27 V at 0.1 rpm (TRW Globe motor, Model 168 A 222 - 4). There are several planetary gear trains to reduce the rpm from the motor shaft value to the shutter speed.

Carbon resistance thermometers are used (Allen - Bradley - Ohmite 39 Ohm, 1/8 Watt). Temperatures are measured upstream and downstream of the plug. The up-stream thermometer T_u is placed in the liquid underneath and sufficiently away from the plug. The downstream thermometer T_d has been mounted within the FCP at its outer radius. A heater (H) permits external supply of heat to the He II upstream of the plug. Pressures are sensed up-stream and downstream (P_u and P_d respectively). The up - stream sense tube is a stainless steel tube of alloy 316 (0.159 cm = 1/16 in., wall thickness 0.025 cm = 0.010 in). It is located 50 cm above the plug outside the liquid bath in order to avoid large hydrostatic pressure changes. The downstream sense tube senses the pressure P_d at a location 0.5 cm above the shutter. The small hydrostatic pressure difference of $g \, \rho_v \, \Delta z \approx 10^{-4}$ milli-bar is

negligible compared to the pressure difference $(P_u - P_d)$; (g gravitational acceleration, ρ_v vapor density, z position coordinate). The difference $(P_u - P_d)$ is displayed on a differential Bourdon gauge (Wallace & Tiernan model 62D-4C-0040D). The pressure above the He II bath is measured with another Bourdon gauge system (Wallace & Tiernan model FA 145 and FA 160 respectively).

Figure 9 represents details of the plug-plate-shutter assembly with associated spring system. Figure 9a is a top view of the flow control plate with its 40 holes. Figure 9b displays the lower stainless steel tube section. This section has an enlarged thickness in the middle which accommodates the plug. At this location, downstream of and above the plug, the inner diameter is 2.41 cm (=.95 in). The shutter is spring loaded. A spring holder is soldered to the inner wall of the tube section using solder of alloy Sn 63 (Kester solder, Litton Systems). In a similar fashion the lower tube section is soldered to the vent tube jacket. The latter is vacuum-insulated. During rotation the inner shaft transmits torque to the teflon shutter via a pin. The shaft is a stainless steel tube of alloy 304, O.D. 0.3175 cm (=1/4 in.) and wall thickness 0.025 cm = 0.010 in.

Disturbances and system anomalies: Oscillations, liquid breakthrough and friction phenomena. Prior to the description of low temperature runs in the design range, some

27

(a)

(b)

VACUUM SPACE

SHAFT

SPRING
HOLDER

SPRING

PIN

TEFLON
SHUTTER

FLOW
CONTROL
. PLATE

FIBRE GLASS
PAPER LAYER
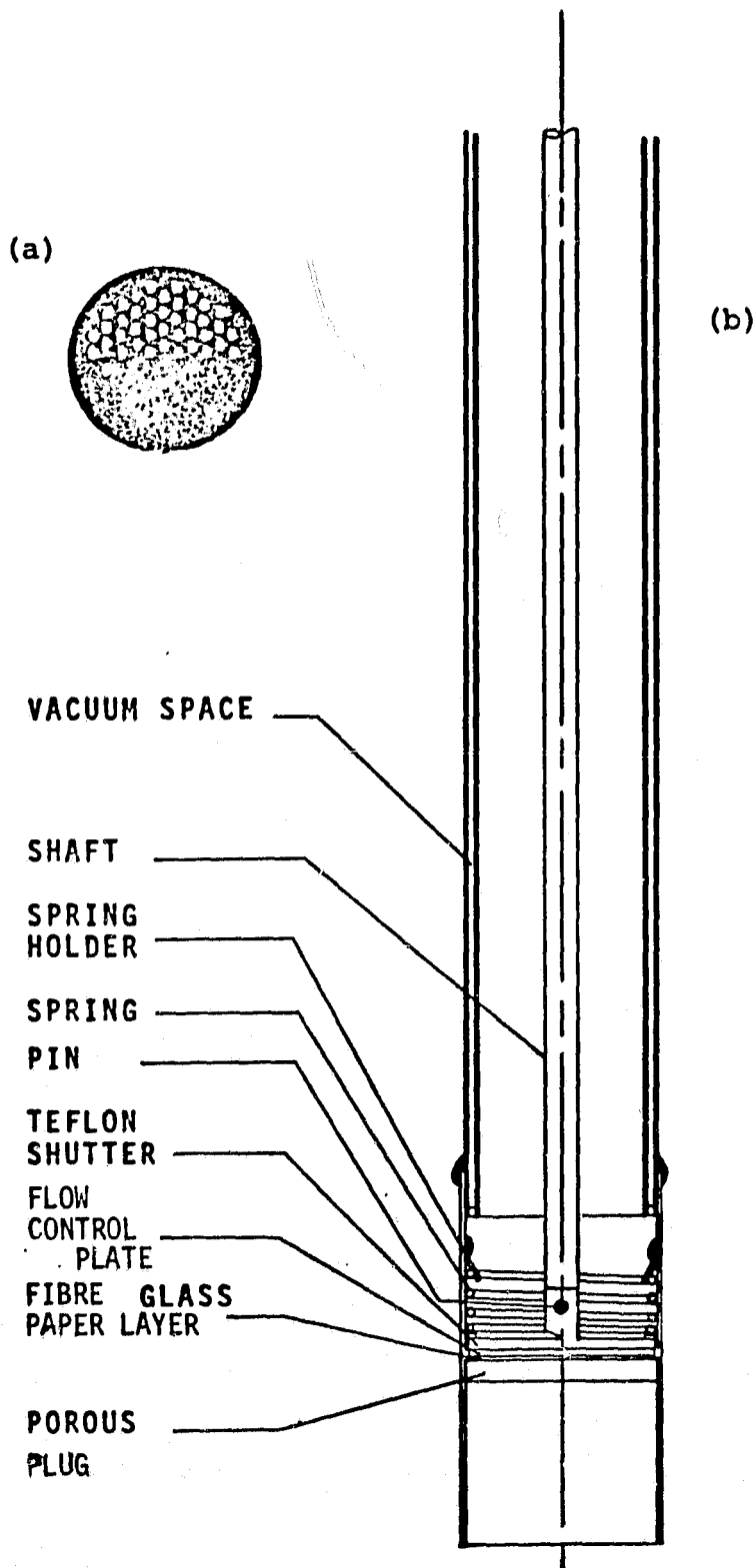
POROUS

PLUG

Figure 9. Details of vapor-liquid phase separator system ;
          a. Flow control plate;
          b. Plug-plate-shutter assembly .

system anomalies are outlined. One case is the lower limit of operation when pressures upstream and downstream are about equal. The other case is friction in the assembly.

When upstream and downstream pumping rates of the terrestrial simulation system are close enough, liquid breakthrough from upstream to downstream may occur. This breakthrough phenomenon is frequently accompanied by oscillations. An example of one type of oscillation is displayed in Figure 10 as temperature T_u versus time t. This case is a consequence of a large system disturbance. The amplitude of T_u is quite large, and there is no clear evidence of a well-defined characteristic frequency.

Another example of oscillations of relatively small amplitude is shown in Figure 11. This type of oscillation may occur when small disturbances are imposed. Concerning ideal theoretical breakthrough conditions , we refer to Appendix A .

Friction is expected to occur as a consequence of contamination of the shutter system. During preparation of the system He^4 gas is used to cover all components immediately after manufacturing. The example shown in Figure 12 depicts an increase in the temperature upon initiation of dissipation due to friction. At the same time temperature fluctuations occur. It is believed that
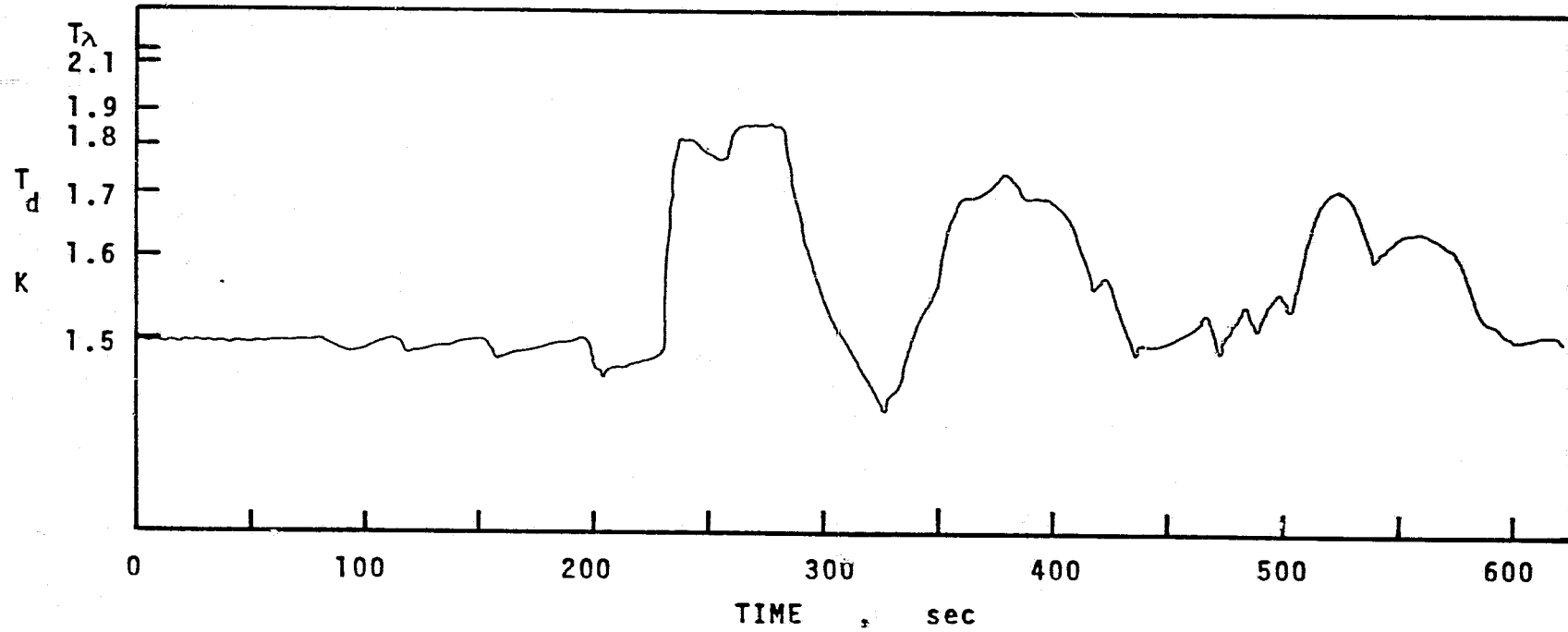
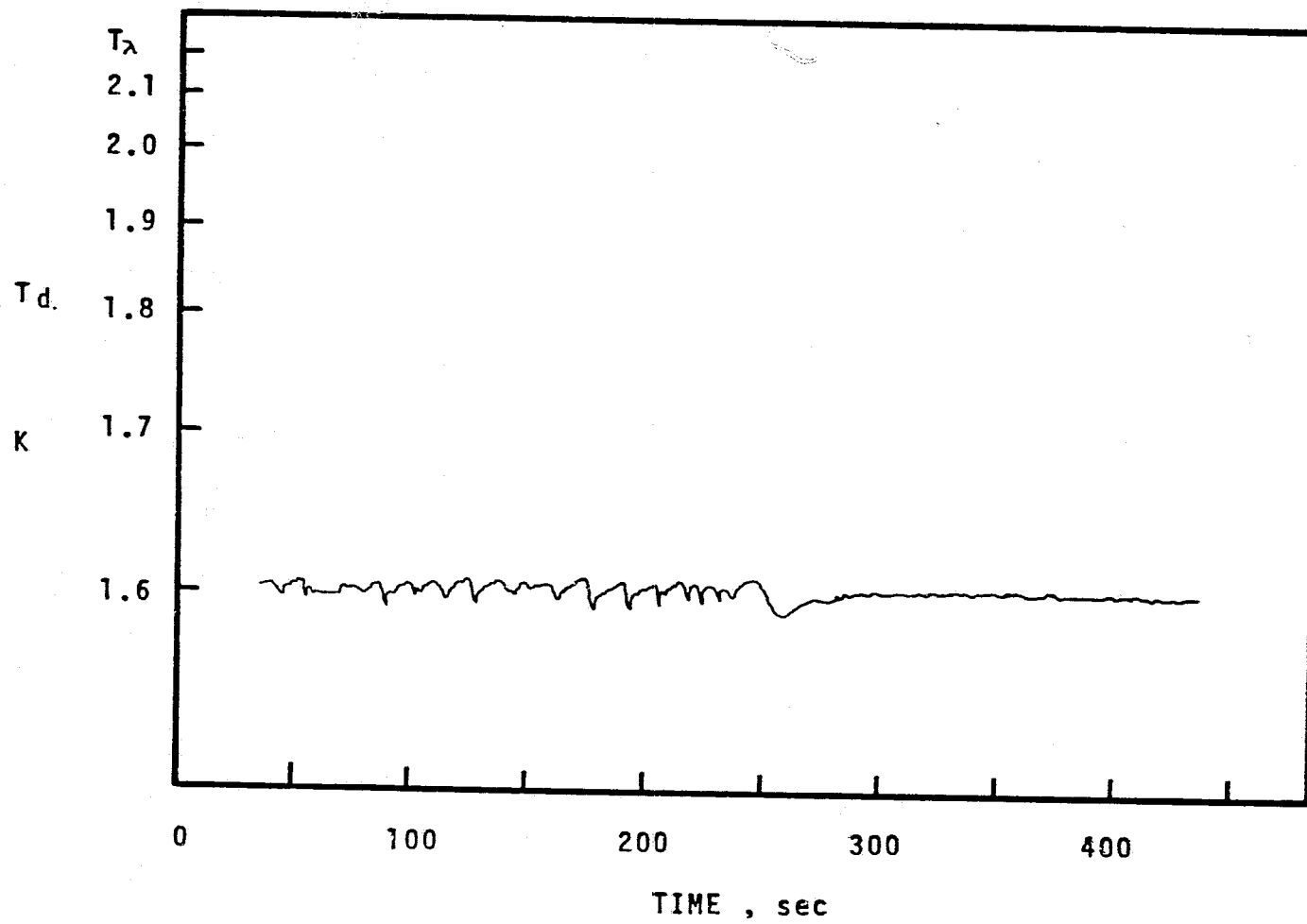Figure 10 . System disturbances sensed by the downstream thermometer.

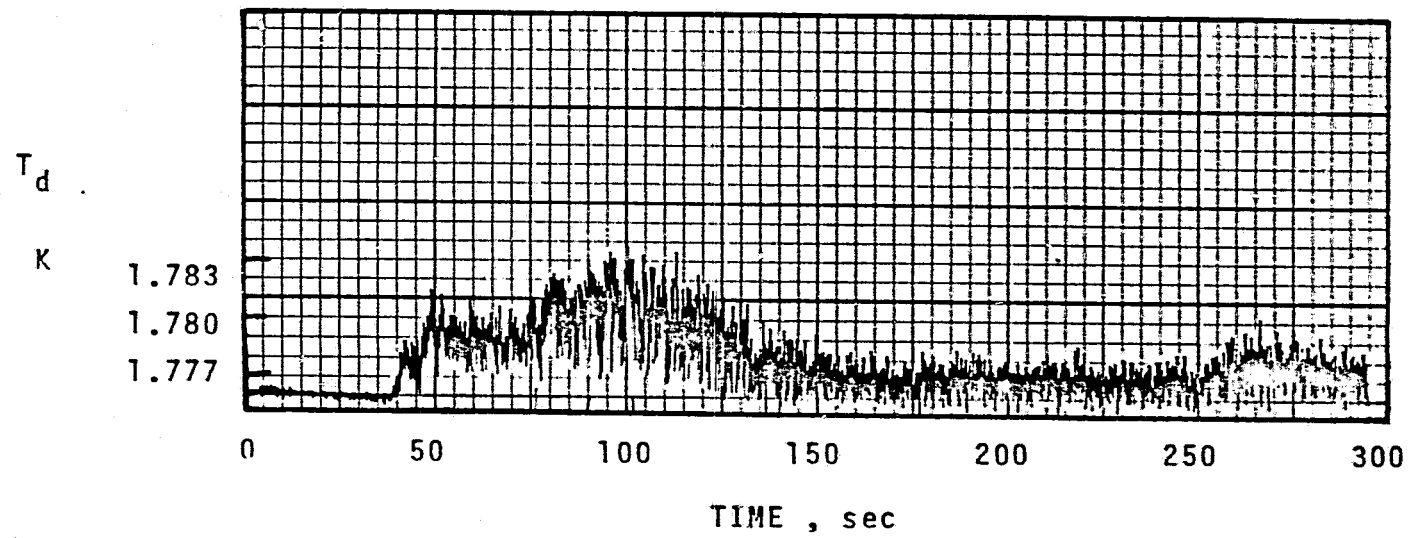Figure 11. Temperature oscillations sensed by the downstream thermometer .

T_d .

K

Figure 12. Signal of downstream thermometer (T_d) versus time during anomaly of operation associated with friction.

this isolated occurrence of friction has been the result
of contamination during a particular warm-up period within
a sequence of experimental runs.

Stationary system properties at low temperature in He II.
Prior to rotation of the shutter system, the plug opera-
tion has been checked for stationary device conditions.
During these runs the position of maximum throughput has
been investigated. After the usual transfer of cryo-liquid
to all cryo-jackets and related precooling , the He I
bath is pumped down toward the lambda point. During this
phase of system preparation upstream bath and downstream
vent duct are connected to bring both sides of the plug
to the lambda temperature. Afterwards, upstream and down-
stream lines are disconnected. This results in a pressure
difference across the plug caused by the downstream pump.
Slow pumpdown toward low temperatures in the He II range
creates quasi-steady transport of heat and mass through
the plug. This requires that the heat capacity terms
are negligible compared to the heat supply rate. The
main contribution during cooldown comes from the He II
bath itself : $\dot{Q}_{transient} = \dot{Q}_{tr} = V_L \rho \cdot C_L \cdot dT/dt$; (V_L =
liquid volume, C_L specific heat per unit mass of liquid,
ρ liquid density)'. The derivative dT/dt has been kept
small enough to satisfy the requirement of quasi-steady
transport. After a particular run , the system is allowed

to warm up toward the lambda temperature. Subsequently another run is started. A particular value of the heater power ($\dot{Q}_{ext}$) is used keeping $\dot{Q}_{ext}$ = const during data collection. Power settings from 50 mW to several 100 mW are covered. In the experiments the upstream side is disconnected from the external equipment, in order to simulate bath conditions of a vessel storing He II.

Figure 13 shows the pressure difference across the plug as a function of the upstream bath temperature. The high throughput provided by the pump at high pressures reflects the behavior of all vacuum pumps known to have been used in this type of simulation test. As the pressure, and with it T_u, is lowered, the pressure difference maintained by the pump diminishes. Finally a limiting low temperature is attained with loss of pumping capability. This temperature is increased as the externally applied heater power is raised. The data are listed in Table V.[2].

Figure 14 permits a comparison of the static pressure difference across the plug with the vapor pressure difference ΔP_v. As discussed in Appendix A, there is a limiting vapor pressure difference ΔP_v. (It depends on the liquid bath depth measured upward from the plug and is a function of the thermophysical properties).

34
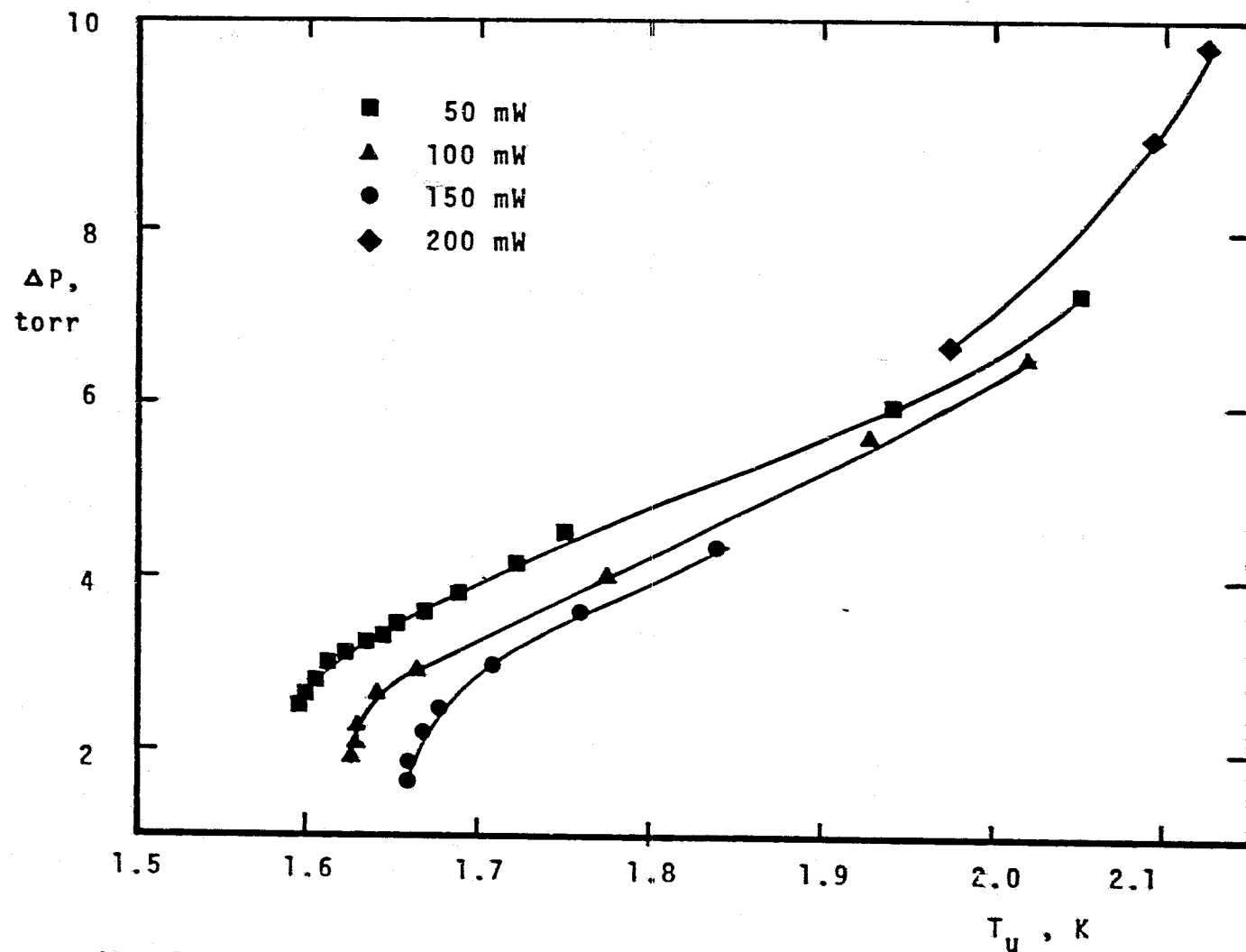
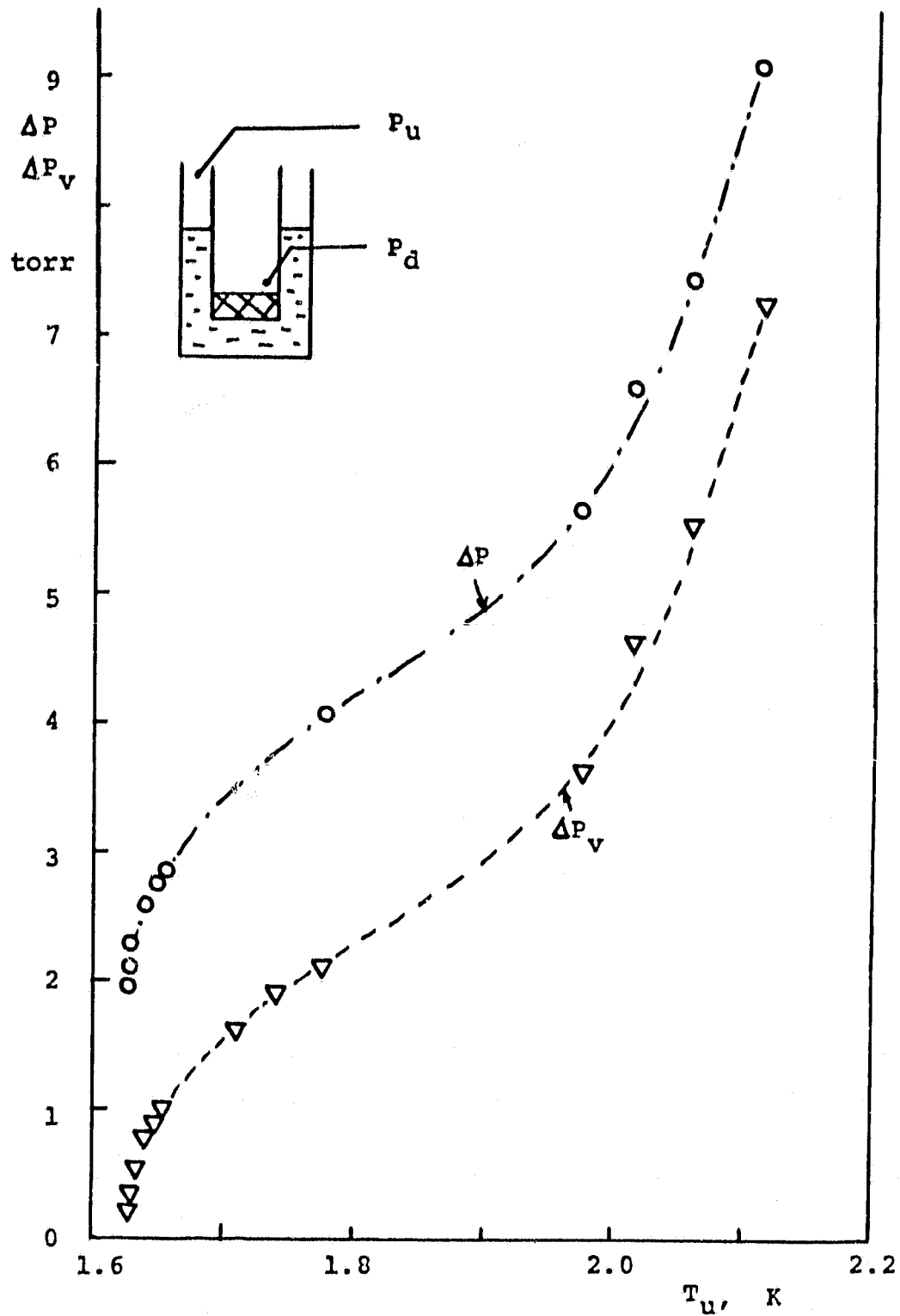Figure 13. Pressure difference across plug for various externally supplied heating rates.

Figure 14. Comparison of static pressure difference ΔP across the plug with the vapor pressure difference $\Delta P_v = (P_u - P_d)$; $(\dot{Q}_{ext} = 100 \text{ mW })$.

TABLE V.2. Data for stationary shutter system at maximum cross sectional area.

$\dot{Q}_{ext}=50$ mW		$\dot{Q}_{ext}=100$ mW		$\dot{Q}_{ext}=150$ mW		$\dot{Q}_{ext}=200$ mW	
T_u, K	ΔP, mb	T_u, K	ΔP, mb	T_u, K	ΔP, mb	T_u, K	ΔP, mb
2.050	9.73	2.015	8.79	1.838	5.81	2.124	13.6
1.94	8.00	1.925	7.51	1.760	4.80	2.092	12.1
1 75	6.00	1.775	5.40	1.710	3.95	1.975	8.87
1.722	5.57	1.665	3.81	1.680	3.35		
1.690	5.12	1.652	3.65	1.669	2.92		
1.669	4.83	1.640	3.48	1.661	2.48		
1.656	4.67	1.632	3.05	1.659	2.17		
1.638	4.36	1.630	2.77				
1.624	4.23	1.629	2.61				
1.616	4.01						
1.608	3.79						
1.603	3.64						
1.595	3.33						

Figure 15 shows the mass flow rate versus time. In the beginning of a particular run, large mass flow rates reflect partially the characteristic conditions of the pumping system. As the time proceeds, the absolute pressure at the plug is lowered more and more . Then the pumping capability decreases. This results in a small derivative $|\dot{dm} / \dot{dt}|$. As the heater power $\dot{Q}_{ext}$, $\dot{m}$ has to increase correspondingly.

Prior to the discussion of proof-of-principle tests some particular conditions of operation of the present stationary system are summarized by listing four points:

1. A finite ΔP_v corresponding to a finite ΔT is required in order to achieve steady and quasi-steady transport in the phase separation mode.

2. The limiting conditions of liquid breakthrough and termination of phase separation depend on the liquid bath depth, pumping rate, and thermophysical properties.

3. A large cross section requires large pumping rates for a specified ΔP_v. For a specified pump throughput, $\dot{Q}_{ext}$ = const, and low T, liquid breakthrough danger is enhanced.

4. During the change of the thermodynamic state from one run to the next, T is raised from a low value to the vicinity of the lambda point. During this change of
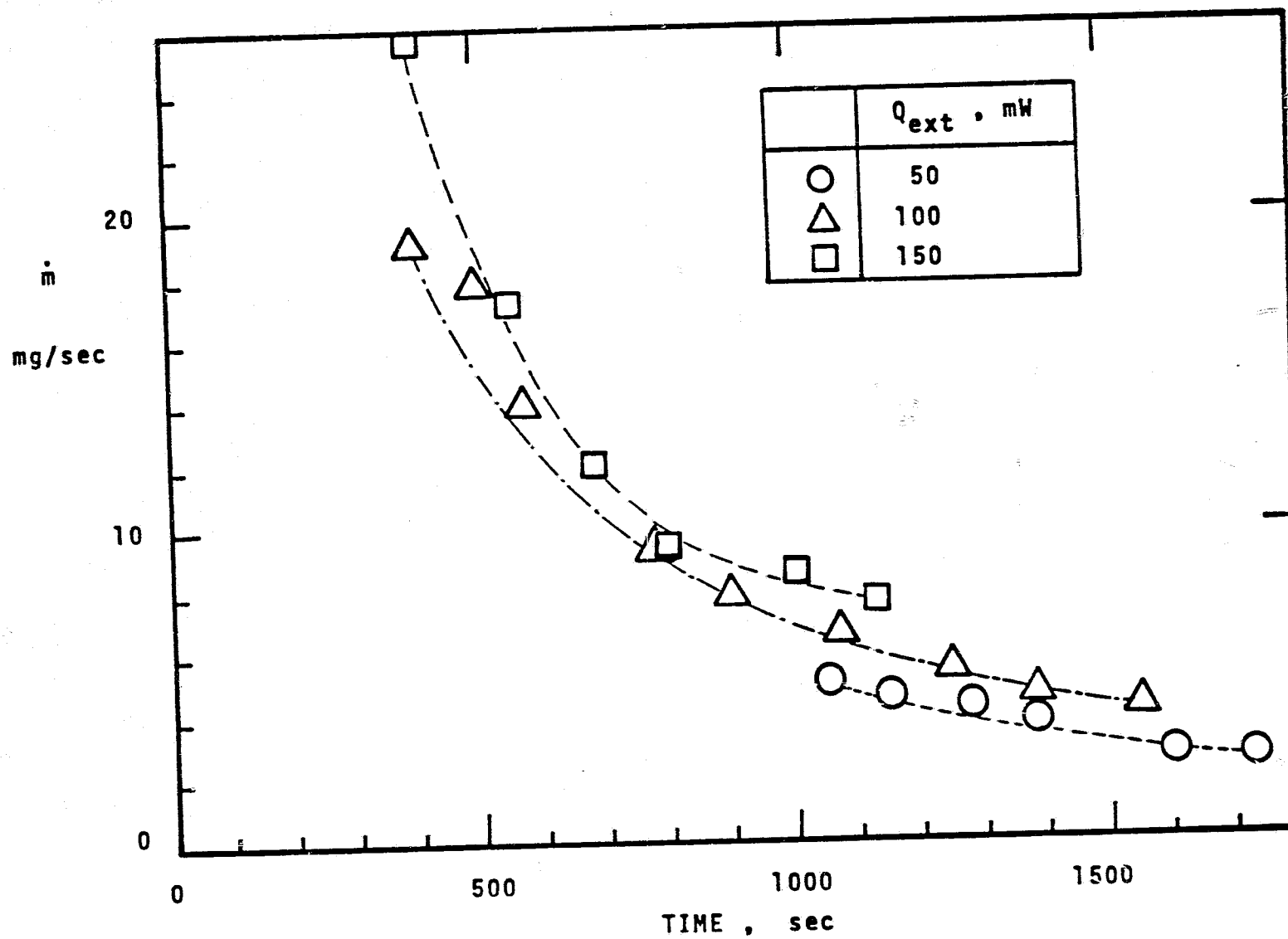
Figure 15. Mass flow rate through the plug as a function of time at various power settings $\dot{Q}_{ext}$.

state the sign of ΔP_v changes resulting in liquid
breakthrough. At the initiation of a new run a
transition, time is needed for the reestablishment
of phase separation.

Proof-of-principle experiments. After the check-out runs
with the stationary system, the motor is switched on
causing a modulation of the cross sectional area available
to the flow . Figure 16 shows the mass flow rate modula-
tion resulting from the rotation of the shutter system .
It is clearly seen that the mass flow rate reaches maxima
and minima. In a particular cycle the maximum occurs when
the shutter system opens up the maximum cross section of
the flow control plate. Afterwards the cross section is
reduced to the minimum value.

For the interpretation of other variables as a
function of time , we note that the rotation is superposed
on the previous quasi-steady cooldown. Figure 17 displays
the upstream bath temperature versus time , and Figure 18
shows the vapor pressure difference ΔP_v (t) .

In Figure 17 the slow cooldown appears to be termi-
nated at T_u close to 1.7 K . Subsequently , a slow rise in
T_u is observed. Details of this rise have not been diag-
nosed, however this phenomenon may be related in part to
pumping limitations when the cross section is opened up.
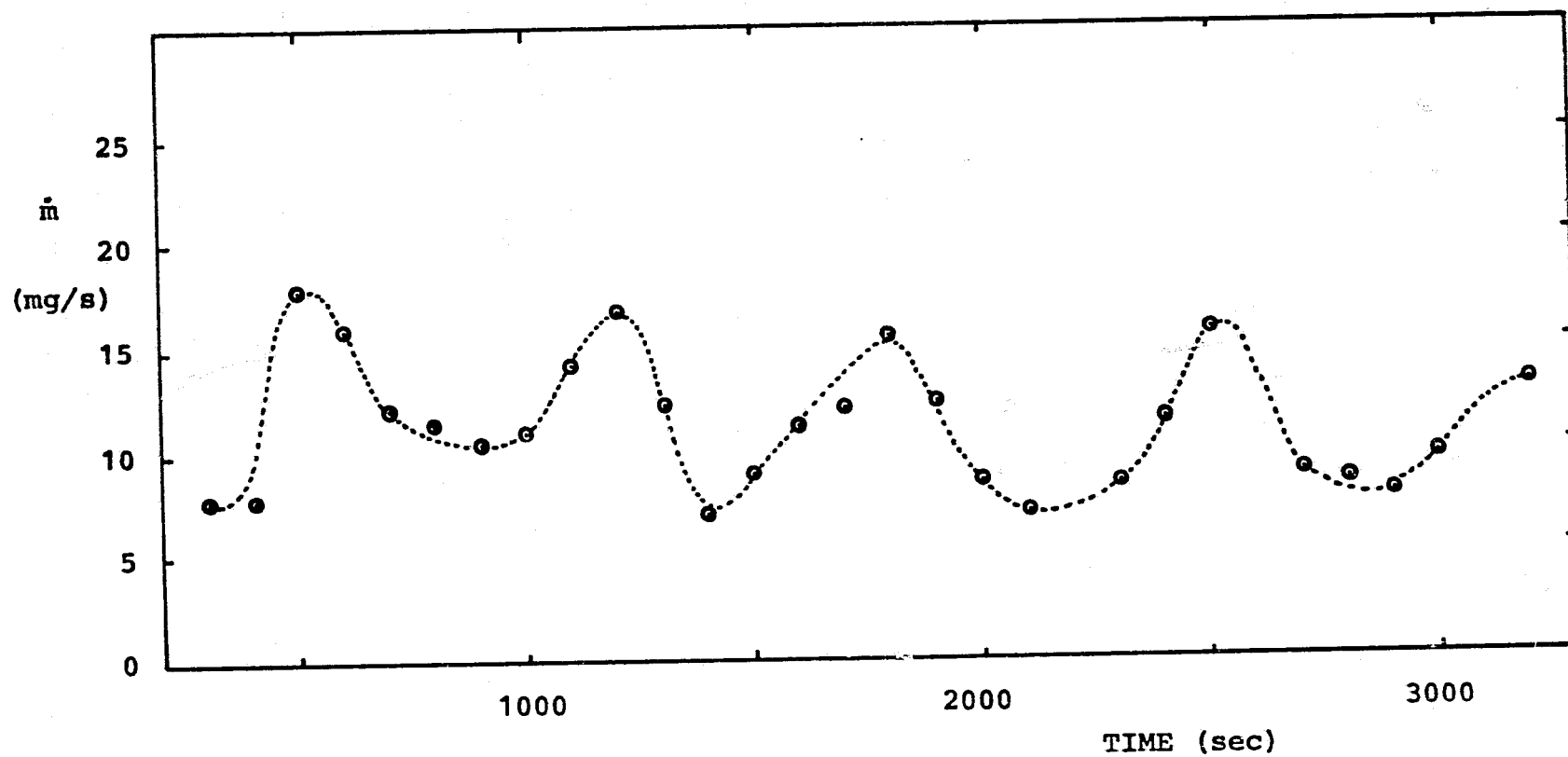During the slow cooldown process, a small derivative

40

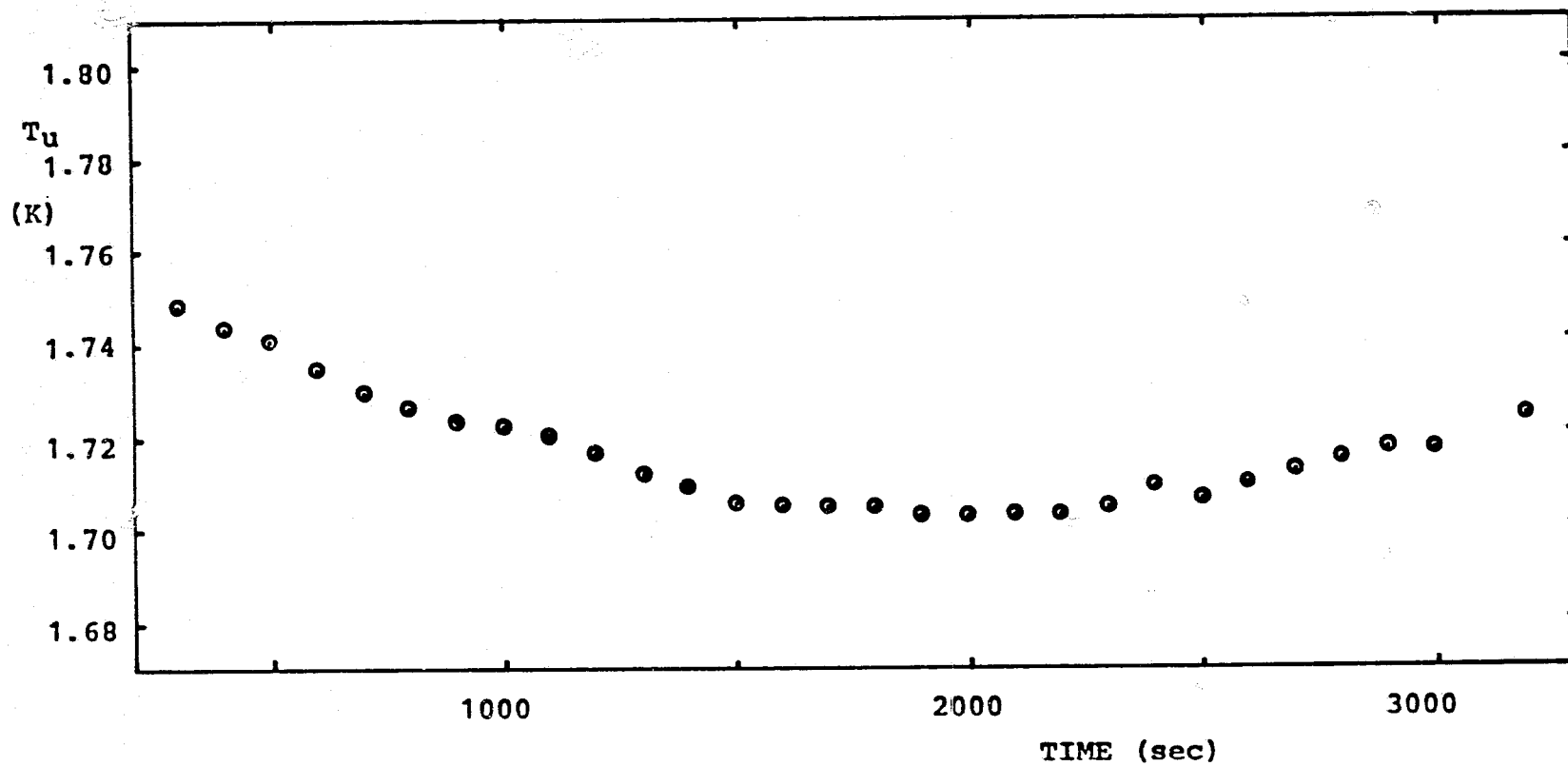Figure 16. Mass flow rate as a function of time during slow rotation of the shutter $(\dot{Q}_{ext} = 50$ mW).

Figure 17 . Upstream temperature T_u of the carbon resistance thermometer as a function of time during slow cooldown and shutter rotation ($\dot{Q}_{ext}$ = 50 mW).
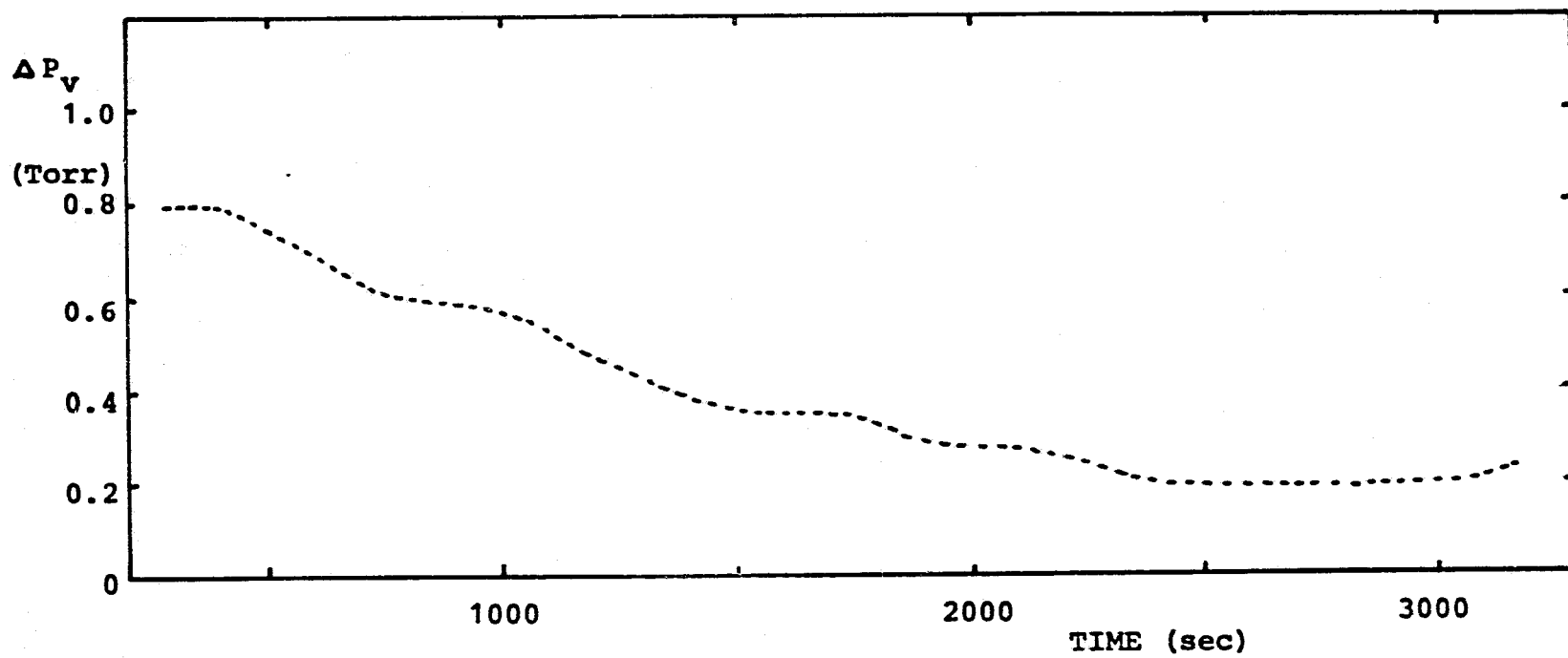
Figure 18 . Vapor pressure difference as a function of time during slow rotation of the shutter ($\dot{Q}_{ext}$ = 50 mW).

dT_u/dt is established when the mass flow rate is near its minimum, i.e. when the flow cross section is covered well by the shutter . A fast change dT_u/dt occurs when the shutter system opens up the flow control plate area to mass and entropy transport. This feature of the system of operation is illustrated in the schematic drawing Figure 19 .
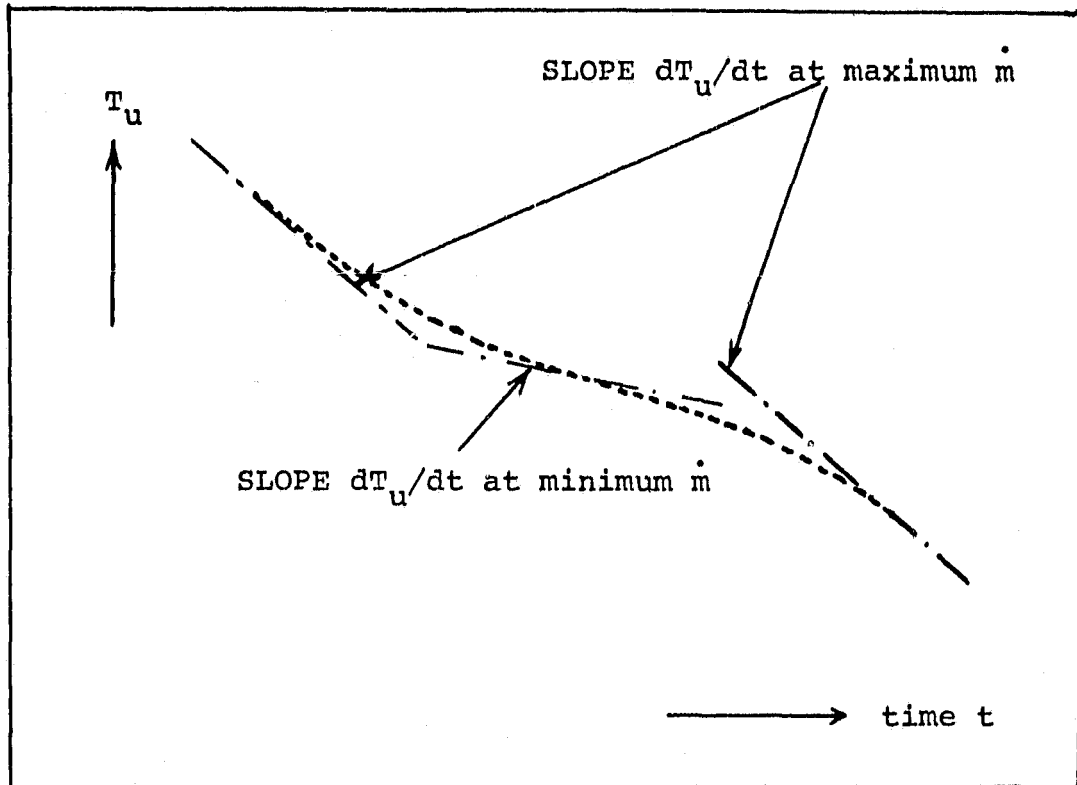

Figure 19. Sketch of temperature variations caused by shutter motion which is superposed upon slow cooldown of the upstream He II bath. $\cdots\cdots$ $T_u = T_u(t)$.

The vapor pressure difference ΔP_v in Figure 18 reflects the cross sectional area variation with time. However this effect is weakened as time proceeds, and as T_u decreases toward its lowest value (Figure 17). When $\dot{m}$ is large , ΔP_v has to be relatively large . This behavior is displayed for the stationary runs in Figure 20 which shows ΔP_v versus $\dot{m}$. As the cross sectional area is reduced during rotation, ΔP_v tends to become smaller. At the same time T_u is lowered. This causes an additional reduction in ΔP_v because of pumping rate limitations associated with the low pump throughput at low pressure. Finally the pumping rate is not sufficient to match shutter rotation requirements. This results in the rise of T_u seen in Figure 17.

Figure 21 shows the bath temperature T_u versus ΔP_v during the slow pumpdown established in the runs with the shutter kept stationary.

Another example of oscillatory mass flow caused by cross sectional area variation in time is shown as Figure 22 for zero externally applied heating power. Thus, only the heat leak of the dewar system has to be rejected via the plug's pores . The resulting mean rate of change of the enthalpy of the He II bath is larger than in the previous case (Figure 16) . Initially high $\dot{m}$-values are established. Subsequently, the mean $\dot{m}$ is reduced as the time t increases. (Because of different liquid bath
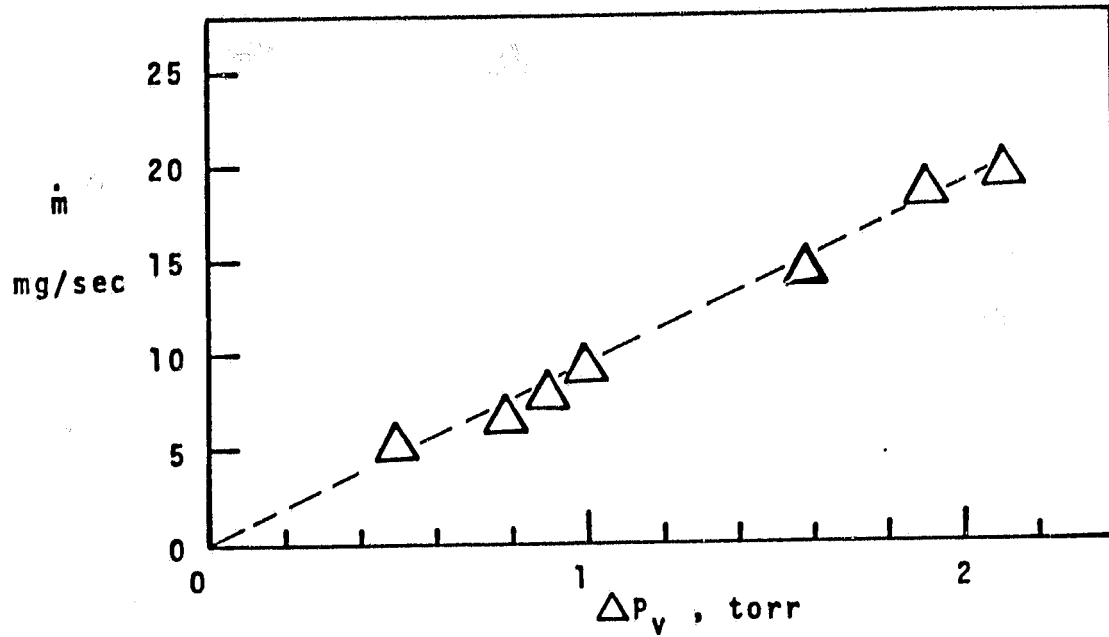
Figure 20. Mass flow rate $\dot{m}$ versus ΔP_v of the stationary plug ; ($\dot{Q}_{ext}$ = 100 mW) .
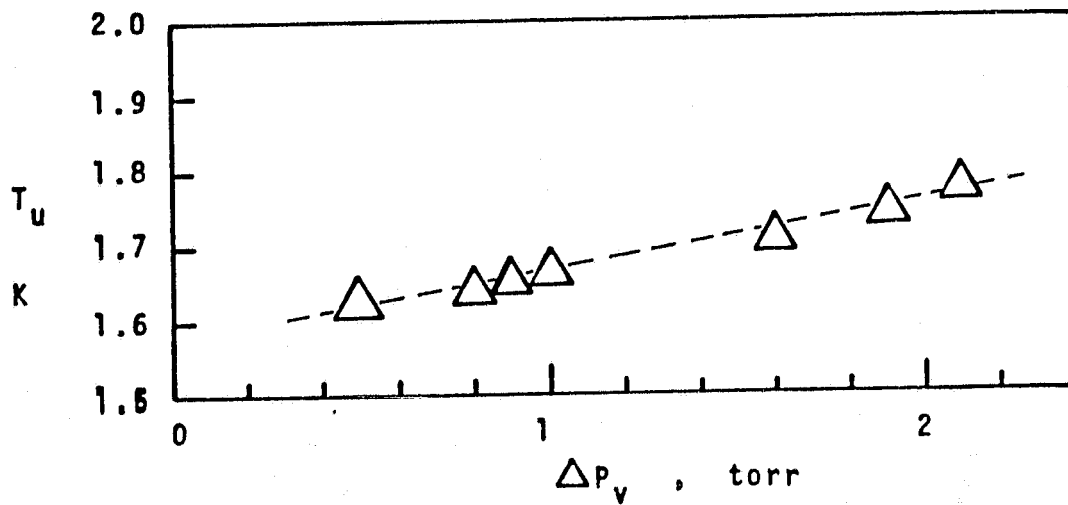

Figure 21. Upstream temperature T_u versus ΔP_v for the data of Figure 20 (stationary plug) ; ($\dot{Q}_{ext}$ = 100 mW).
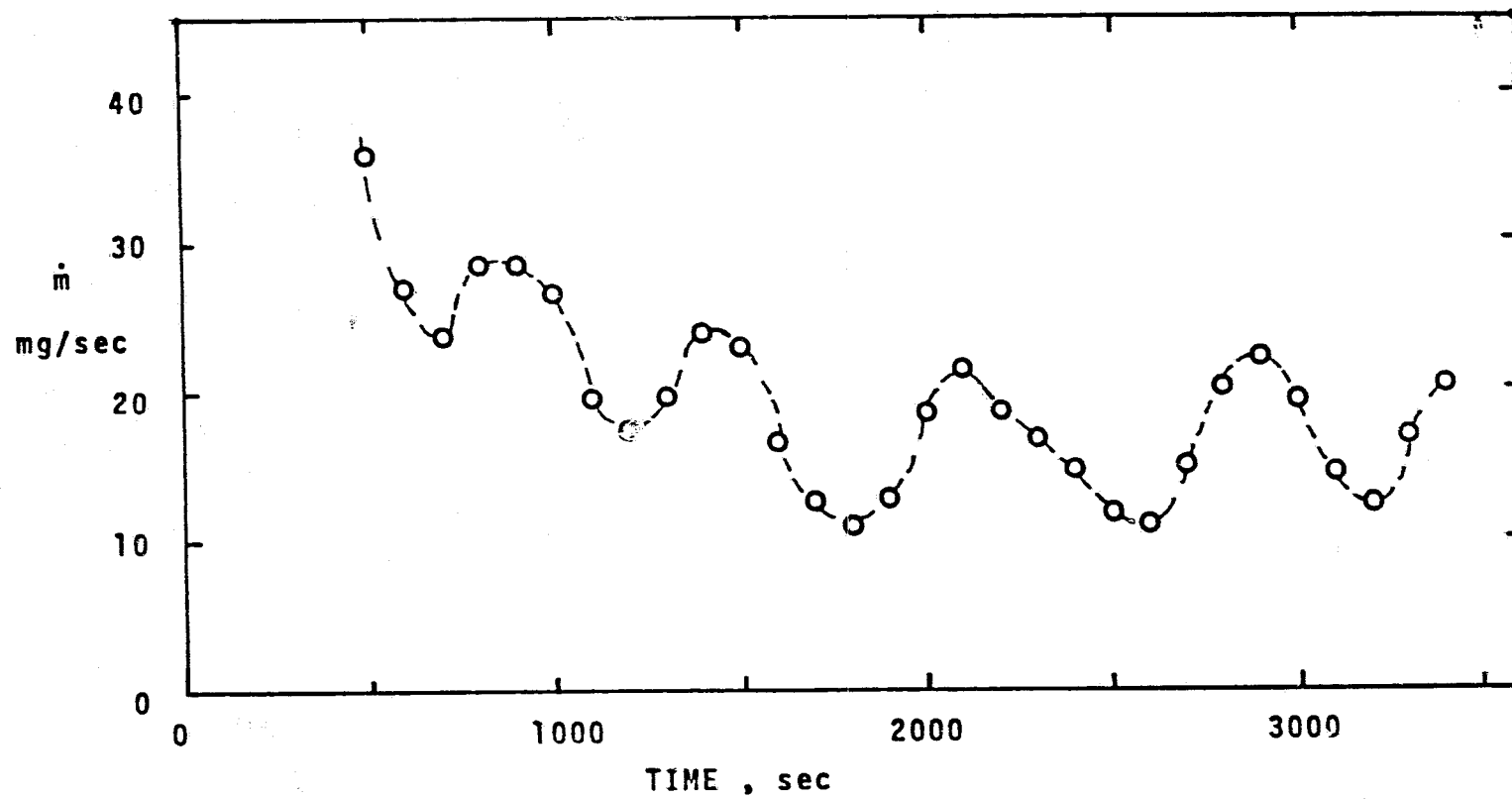
Figure 22. Mass flow rate ṁ versus time during slow rotation of the shutter ($\dot{Q}_{ext} = 0$) .

depths, the static difference ΔP of Fig. 22 differs from the value of Figure 16). The comparison of Figure 22 with Figure 16 shows that the flow rate modulation by the rotating system is established despite transient operation of the He II bath with $dT_u < 0$.

VI. DISCUSSION AND CONCLUSIONS

Major points of the present work are summarized in this section be referring to the stationary shutter system and the variable-area system.

Stationary shutter system. The results obtained are consistent with other porous plug data taken during terrestrial simulation of He II storage in space at reduced gravity forces. Data consistency however extends only to qualitative features related to matching of the pump throughput function to the plug performance function, e.g. pressure drop versus mass flow rate. The stainless steel data appear to differ quantitatively from other sintered systems, such as porous tungsten or ceramic plugs.

Rotating shutter system . No comparable data appear to be available in the literature. The present vapor-liquid phase separator with variable cross sectional area does indeed permit substantial changes in the throughput rate of the system. Thus, the design goal has been realized with a relatively simple device which takes care of varying heat loads of the He II storage vessel. No liquid breakthrough occurs in the range of operation as long as the pumping rate matches the cross sectional area variations established.

<u>Conclusions</u>. It is concluded that variable-area devices, such as the present shutter system, may handle variations of mass and entropy throughputs required for He II systems subjected to variable heat inputs. Modifications which belong to the same family of devices may be employed when different specifications are imposed. An example is a plug system with n plugs (e.g. n = 4 in Section III, Figure 2). This may serve even for the introduction of asymmetries in the time-varying throughput function $\dot{m}(t)$. The latter is close to an even function in the present system.

It is emphasized that precautions are required to prevent contamination of the system during preparation and operation at low temperatures. Further, it is noted that this type of system is not applicable, in unmodified form, for use as a shut-off valve due to danger of liquid breakthrough at very small cross sectional area.

REFERENCES

1. J.W. Vorreiter, Proc. ICEC-7, London 1978, IPC
   Sci. Technology Press, Guildford 1978,p.1

2. H.D. Denner, I. Klipping, J. Menzel, G. Klipping,
   K. Luders and U. Ruppert, Proc. ICEC-7, IPC
   Sci. Technology Press, Guildford 1978,p. 240.

3. H.D. Denner, G. Klipping, I.Klipping, K. Luders,
   J. Menzel, U. Ruppert and H. Walter, ICEC-8,
   Genova 1980, paper 2G-4.

4. A.E. Scheidegger,"The Physics of Flow Through
   Porous Media", Univ. Toronto Press 1974.

5. R.E. Collins," Flow of Fluids Through Porous
   Materials", Reinhold, New York, 1961.

6. Y.I. Kim, C. Chuang and T.H.K. Frederking,"Cryog.
   Processes and Equipment in Energy Systems ",
   ASME , New York, 1980; (Century II Publ.)p.135.

7. H.D. Denner, G. Klipping, I. Klipping, J. Menzel
   and U. Ruppert, Cryogenics 18, 166 (1978).

8. G.R. Karr and E.W.Urban, Cryogenics 20, 266 (1980).

9. E.W. Urban, L. Katz and G.R. Karr, Proc. LT-14,
   North Holland, Amsterdam 1975, Vol.4,p.37.

10. D. Petrac and P.V. Mason, Proc. ICEC-7, London 1978
    IPC Sci. Technol. Press, Guildford 1978,p.120.

11. S.C. Soloski, S. Caspi, Y.I. Kim, C. Chuang and
    T.H.K. Frederking, Rept. UCLA-ENG-7946.

12. R.B. Hall, M.Sc. thesis, Univ. Calif. , Los Angeles
    1967.

13. A.T. Robinson, Trans. ASM 57, 650 (1964).

APPENDIX A

LIQUID BREAK-THROUGH CONDITIONS FOR IDEAL THERMOSTATIC SYSTEM

Consider the thermostatics of the bath configuration depicted in Figure A.1 . The vapor pressure difference is assumed to be $(P_u - P_d) > 0$. with $H_u > 0$. In general the hydrostatic pressure difference ΔP_g may be smaller than , equal to , or larger than the thermo-osmotic pressure difference

$$\Delta P_T = \int \rho \, S \, dT = \overline{(\rho S)} \cdot \Delta T \qquad (A.1)$$

The hydrostatic difference is

$$\Delta P_g = g \, \rho \, H_u \qquad (A.2)$$

In order to achieve separation of liquid He II from its vapor, one has to avoid liquid breakthrough, i.e. very small pressure differences ΔP_T have to be avoided. To be on the safe side, one also has to rule out equality of the differences (A.1) and (A.2). Thus, the requirement of safe operation in terrestrial tests has to be
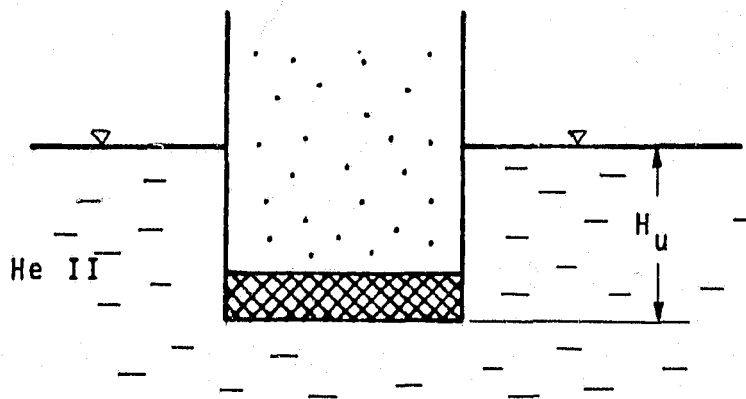

Figure A.1.

Liquid configuration of simulation experiment.

$$\Delta P_T > (\Delta P_g + \Delta P_v) \qquad\qquad (A.3)$$

In this equation the vapor pressure difference is available in terms of the temperature difference (e.g. via T-58). The special case of very small ΔT may be of some relevance . As $\rho_v \ll \rho_{Lsat}$, the Clausius - Clapeyron equation reduces to

$$\Delta P_v / \Delta T = \rho_v \lambda / T \qquad ; \qquad\qquad (A.4)$$
$$\Delta T \ll T$$

(λ latent heat of vaporization, ρ_{Lsat} = density of saturated liquid $\to \rho$). On the basis of Equations (A.2), (A.3) and (A.4), requirement (A.3) is rewritten as

$$\Delta P_v > \frac{g \rho H_u}{\left[\dfrac{\rho S T}{\rho_v \lambda} - 1\right]} \qquad\qquad (A.5)$$

where the ratio of the two pressure differences is

$$\frac{\Delta P_T}{\Delta P_v} = \frac{\rho S T}{\rho_v \lambda} \qquad ; \qquad \Delta T \ll T \qquad (A.6)$$

(This ratio is of the order of magnitude 10 in the range considered). Similarly the required temperature difference may be written as

$$\Delta T > \frac{g H_u}{S \cdot \left[1 - \dfrac{\rho_v \lambda}{\rho S T}\right]} \qquad ; \qquad\qquad (A.7)$$
$$\Delta T \ll T$$

In general there are three thermo-static (ideal) cases:for a specified temperature difference :

a. H_u greater than the limiting theoretical value at the onset of liquid breakthrough ;

b. H_u equal to the limiting value at the onset of liquid breakthrough;

c. H_u is smaller than the limiting value,i.e.there is safe operation of the phase separator in the vapor-liquid separation mode.

These three cases are displayed in the pressure - temperature diagram (Figure A.2).
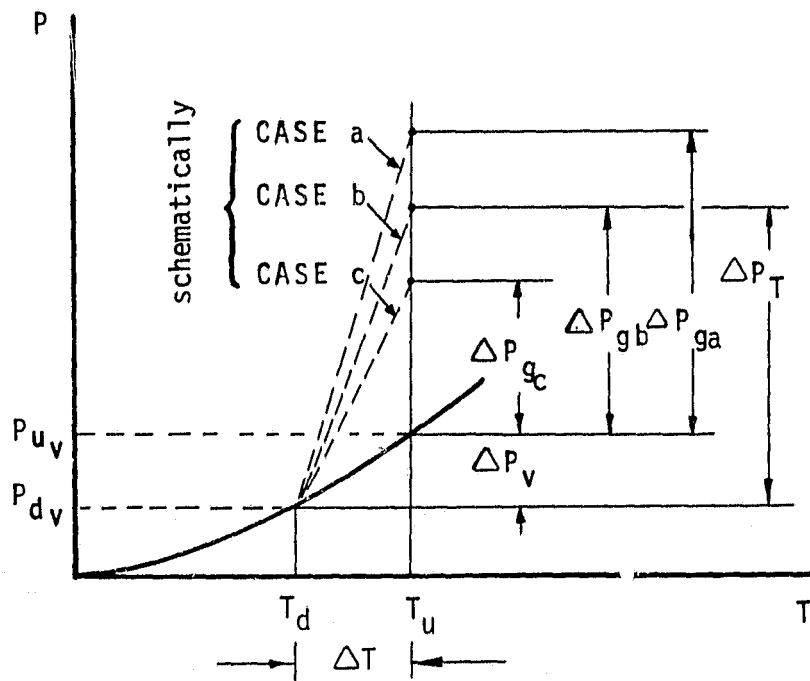

Figure A.2 . Pressure - temperature diagram (schematically)

The order of magnitude of the temperature difference at the theoretical limit (inequality sign of A.7 changed to equality sign) is illustrated. For S of the order of 10^6 cgs units, g of the order 10^3 and H_u of the order 10 cm , and the expression in brackets of the denominator is 1 , the temperature difference has the order of magnitude 10 milli- K .

At reduced gravity the forces may be characterized by an acceleration $a = x g$ with $x < 1$. In this case the gravitational acceleration g in the preceding equations has to be replaced by xg. The danger of liquid breakthrough is lowered considerably for $x \ll 1$.